

Chapter 3:

RESULTS

Section 3.1:

***In silico* and expression analyses of Fae in**

M. oryzae

Section 3.1: *In silico* and expression analysis of Fae in *M. oryzae*

This section describes the initial identification of putative *FAEs* in the genome of *M. oryzae* and a phylogenetic analysis of Fae across different host-specific isolates of *M. oryzae* and in various other fungal species. Further, the secretory nature of the Fae was studied too. Since most of the CWDEs are generally found to be under tight genetic regulation, the expression pattern of *FAE* was analysed under both *in vitro* and *in vivo* conditions. Altogether, this analysis provided an insight into evolutionary aspects of Fae and its important role in pathogenicity of *M. oryzae*.

3.1.1 Identification of putative *FAEs* in *M. oryzae* by *in silico* analysis

A protein BLAST analysis was performed using the known type B Fae sequences from *Aspergillus oryzae* (AoFaeB; PDB: 3WMT_B) and *Neurospora crassa* (NcFaeB; GenBank: AJ293029) as a query against *M. oryzae* 70-15 reference genome database. A total of nine putative feruloyl esterases were found in *M. oryzae* genome that showed homology with either AoFaeB or NcFaeB (Table 3.1.1). While MGG_08737 and MGG_07294 showed highest (47% and 75%) identity to AoFaeB and NcFaeB, respectively, MGG_03771 showed similarity to both the reference sequences (Table 3.1.1).

Gene ID	Protein BLAST	
	<i>E-value</i>	<i>Identity</i>
MGG_07294.6	8e-157	75.37% to NcFaeB
MGG_08737.6	6e-170	47.47% to AoFaeB
MGG_03771.6	1e-165 0.42	45.88% to AoFaeB, 33.33% to NcFaeB
MGG_09404.6	7e-135	40.47% to AoFaeB
MGG_05529.6	1e-79	34.3% to AoFaeB
MGG_03502.6	2e-75	31.59% to AoFaeB
MGG_05366.6	4e-67	29.55% to AoFaeB
MGG_02261.6	9e-67	32.01% to AoFaeB
MGG_09732.6	2e-29	24.95% to AoFaeB

Table 3.1.1: List of putative Fae sequences obtained from *M. oryzae* database upon protein BLAST analysis using AoFaeB or NcFaeB.

It has been reported that feruloyl esterases belong to the α/β -hydrolase-fold superfamily and catalyze substrate hydrolysis following the mechanism of serine proteases with a conserved GX SXG motif and Ser-His-Asp/Glu catalytic triad (Dilokpimol et al., 2016). To check for the presence of this conserved motif, a multiple sequence alignment of all nine putative Fae in *M. oryzae*, along with a AoFaeB and NcFaeB, was performed using ClustalW feature in MEGA tool. Sequence comparison showed the presence of the conserved GX SXG motif in all the nine Fae proteins in *M. oryzae* (Fig. 3.1.1). Similarly, Fae in *M. oryzae* were found to belong to α/β hydrolase-fold superfamily, as checked using the NCBI conserved domain database (<http://www.ncbi.nlm.nih.gov/Structure/cdd/wrpsb.cgi>; Marchler-Bauer et al., 2015).

3.1.3 Phylogenetic analysis of *M. oryzae* Fae with other fungal Fae

A characteristic feature of feruloyl esterases is the presence of Tannase or Esterase conserved domain. Here, an hmm-based search was performed to check for the presence of the Tannase (Pfam ID: PF07519.13) or Esterase_PHB (Pfam ID: PF10503.13) domain within the Fae protein sequences of *M. oryzae*. Although, nine *M. oryzae* Fae share relatively low sequence homology with each other (section 3.1.2), they showed presence of either of the conserved domains (Table 3.1.2). However, the *M. oryzae* genome, unlike in the GX SXG motif-based analysis (section 3.1.1), showed twelve putative Fae sequences, wherein nine (MGG_03771, MGG_03502, MGG_05366, MGG_02261, MGG_05592, MGG_08737, MGG_09404, MGG_09677 and MGG_09732) contained Tannase and the rest three (MGG_03746, MGG_07294 and MGG_10618) had Esterase_PHB domain.

For a wider/broader phylogenetic analysis, hmm-based search for the presence of Tannase or Esterase_PHB domain was performed within the Fae protein sequences of twenty-six representative fungi, including *M. oryzae* (70-15), belonging to nine different taxonomic classes and fifteen orders. A total of 215 putative Fae protein sequences were found in these fungi, of which 149 showed the presence of Tannase domain, whereas the remaining 66 protein sequences contained an Esterase_PHB domain (Table 3.1.2). Interestingly, majority of the phytopathogenic fungi such as *Fusarium spp.*, *V. mali*, *Magnaporthe spp.*, *Colletotrichum graminicola* and *Zymoseptoria tritici* showed more than one Tannase-domain-containing, highly-variable Fae sequences. However, *Ustilago maydis*, a basidiomycete causal agent of corn smut disease, showed only two Esterase_PHB domain containing Fae sequences. Intriguingly, the non-phytopathogenic filamentous fungi such as *N. crassa*, and particularly *Aspergillus spp.*, also showed more than one putative FAE in

their genomes, whereas fission yeast (*S. pombe*) or budding yeast (*S. cerevisiae*) did not show any Fae sequence.

Table 3.1.2: Number of putative feruloyl esterases (Fae), with Tannase or Esterase_PHB domain, identified species.

Fungal Species	Fungal Class	Assemblies Accession	Number of putative Fae		
			Tannase Domain	Esterase_P HB Domain	
<i>Alternaria alternata</i>	<i>Dothideomycetes</i>	GCF_001642055.1	8	6	plant pathogen; cause
<i>Aspergillus fumigatus</i>	<i>Eurotiomycetes</i>	GCF_000002655.1	5	4	non-pathogenic to pl
<i>Aspergillus nidulans</i>	<i>Eurotiomycetes</i>	GCF_000149205.2	8	3	saprophytic fungus; c
<i>Aspergillus niger</i>	<i>Eurotiomycetes</i>	GCF_000002855.3	23	2	causes black mold di
<i>Aspergillus oryzae</i>	<i>Eurotiomycetes</i>	GCF_000184455.2	11	2	non-pathogenic to pl
<i>Coccidioides immitis</i>	<i>Eurotiomycetes</i>	GCF_000149335.2	0	1	causal agent of valley
<i>Colletotrichum graminicola</i>	<i>Sordariomycetes</i>	GCF_000149035.1	10	6	plant pathogen; cause
<i>Cryptococcus neoformans</i>	<i>Tremellomycetes</i>	GCF_000091045.1	0	0	non-pathogenic to pl
<i>Eremothecium cymbalariae</i>	<i>Saccharomycetes</i>	GCF_000235365.1	0	0	non-pathogenic; used
<i>Fusarium graminearum</i>	<i>Sordariomycetes</i>	GCF_000240135.3	7	6	plant pathogen; cause
<i>Fusarium oxysporum</i>	<i>Sordariomycetes</i>	GCF_000149955.1	10	6	plant endophytes or s
<i>Gaeumannomyces tritici</i>	<i>Sordariomycetes</i>	GCF_000145635.1	12	4	plant pathogen; cause
<i>Histoplasma capsulatum</i>	<i>Eurotiomycetes</i>	GCF_000149585.1	0	0	non-pathogenic to pl
<i>Magnaporthe poae</i>	<i>Sordariomycetes</i>	GCA_000193285.1	9	2	plant pathogen; cause
<i>Magnaporthe grisea</i>	<i>Sordariomycetes</i>	GCF_004355905.1	10	4	plant pathogen; cause
<i>Magnaporthe oryzae</i>	<i>Sordariomycetes</i>	GCF_000002495.2	9	3	plant pathogen; cau
<i>Mucor lusitanicus</i>	<i>Mucormycetes</i>	GCA_010203745.1	0	0	non-pathogenic to pl
<i>Neurospora crassa</i>	<i>Sordariomycetes</i>	GCF_000182925.2	1	4	non-pathogenic to pl
<i>Pyricularia pennisetigena</i>	<i>Sordariomycetes</i>	GCF_004337985.1	9	2	pathogenic to signal
<i>Saccharomyces cerevisiae</i>	<i>Saccharomycetes</i>	GCF_000146045.2	0	0	non-pathogenic
<i>Schizosaccharomyces pombe</i>	<i>Schizosaccharomycetes</i>	GCF_000002945.1	0	0	non-pathogenic
<i>Sclerotinia sclerotiorum</i>	<i>Leotiomycetes</i>	GCF_000146945.2	3	1	plant pathogen; cause
<i>Ustilago maydis</i>	<i>Ustilaginomycetes</i>	GCF_000328475.2	0	2	plant pathogen; cause
<i>Valsa mali</i>	<i>Sordariomycetes</i>	GCA_000818155.1	2	1	plant pathogen; cause
<i>Verticillium dahlia</i>	<i>Sordariomycetes</i>	GCF_000150675.1	6	5	plant pathogen; cause
<i>Zymoseptoria tritici</i>	<i>Dothideomycetes</i>	GCF_000219625.1	6	2	plant pathogen; cause
Total			149	66	

Further, the phylogenetic tree showed that Fae sequences had a significant genetic diversity and a discontinuous distribution pattern even among multiple Fae of the same species (Fig. 3.1.3). All the clades, except for clade E and F, contained Fae sequences from species belonging to more than one taxonomic class. Whereas Fae sequences from clades E and F were found to be unique to class *Sordariomycetes* (Fig. 3.1.3). All, except one, Fae sequences in clade E comprised of fungi predominantly belonging to the order *Magnaporthales*. Importantly, four out of nine putative Fae from *M. oryzae* (viz. MGG_02261, MGG_03502, MGG_05366 and MGG_05592), along with that from *N. crassa*, were grouped in clade E. The remaining five *M. oryzae* Fae orthologs were found to be grouped together in clades B, C, G and I with that from either of the distantly related genera like *Fusarium*, *Colletotrichum* or *Aspergillus* as compared to their absence in a taxonomically closely related species *N. crassa*, suggesting a likely loss/reduction of Fae genes in the non-phytopathogenic fungus. Interestingly, out of the nine Tannase domain containing *M. oryzae* Fae, MGG_08737 (depicted as red star in Fig. 3.1.3) was found to be highly diverged.

Altogether, absence of any putative Fae in budding and fission yeasts or human fungal pathogens (such as *Cryptococcus neoformans*, *Coccidioides immitis*, *Histoplasma capsulatum* and *Mucor lusitanicus*) suggests that the enzyme from other, especially phytopathogenic, fungal species is mainly associated with degradation of plant cell walls. Similarly, presence of large number of Fae sequences in non-phytopathogenic filamentous fungi such as *Aspergillus spp.* and *N. crassa* is intriguing, and further studies on *FAEs* across different fungal genera could possibly shed some light on any evolutionary aspect of it.

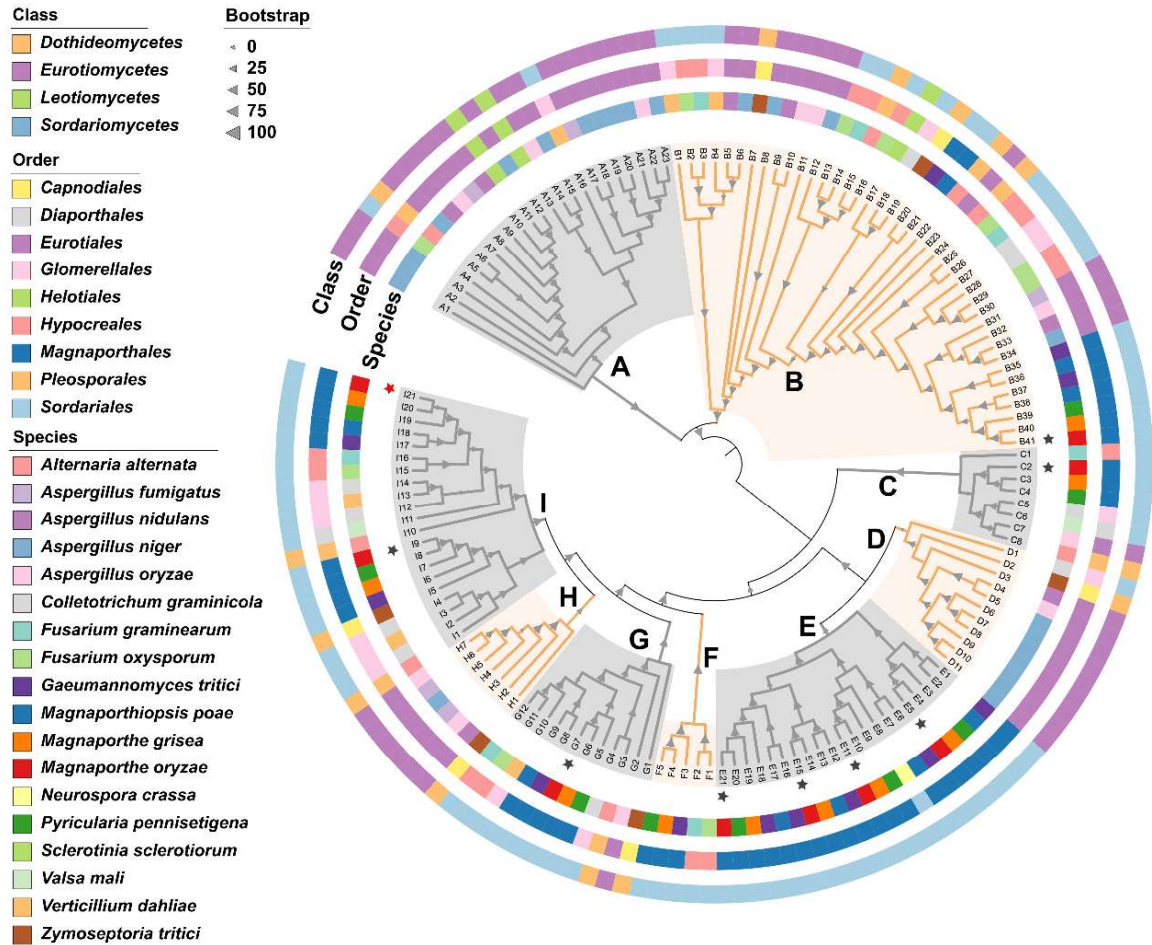


Figure 3.1.3. Phylogenetic analysis of Fae sequences from 18 fungal species representing four classes. The mid-point rooted phylogenetic tree is based on maximum likelihood methods, with assessment of branch support by 1000 bootstrap replicates. Tree branches are color-coded according to the specific fungal species. The colors in the outer, middle and inner circular strips represent taxonomy, for each branch, with respect to fungal class, order and species, respectively. Bootstrap values are indicated as grey triangles, sized according to the values. Letters in upper-case from A to I denote the major clades of the tree. Stars denote Fae proteins from *M. oryzae*; red-colored star marks the MGG_08737 gene used in the present study. Stars in clockwise direction, corresponding to leaf labels B41, C2, E5, E11, E15, E21, G7, I9 and I21 denote putative Fae encoded by MGG_09677, MGG_09732, MGG_03502, MGG_02261, MGG_05592, MGG_05366, MGG_09404, MGG_03771, and MGG_08737, respectively. A detailed information of the leaf-labels for each major clade, along with the respective protein IDs can be found in Table 3.1.3.

Major Clades	Leaf labels	Protein IDs	Domain Position	Species	Order	Class
A	A1	XP_001388709.1	73-572	<i>Aspergillus niger</i>	Eurotiales	Eurotiomycetes
	A2	XP_001389868.1	71-549	<i>Aspergillus niger</i>	Eurotiales	Eurotiomycetes
	A3	XP_001396513.1	72-559	<i>Aspergillus niger</i>	Eurotiales	Eurotiomycetes
	A4	XP_018257870.1	70-564	<i>Fusarium oxysporum</i>	Hypocreales	Sordariomycetes
	A5	XP_018383515.1	78-574	<i>Alternaria alternata</i>	Pleosporales	Dothideomycetes
	A6	XP_001402486.1	72-564	<i>Aspergillus niger</i>	Eurotiales	Eurotiomycetes
	A7	XP_660301.1	85-559	<i>Aspergillus nidulans</i>	Eurotiales	Eurotiomycetes
	A8	XP_001826685.1	71-572	<i>Aspergillus oryzae</i>	Eurotiales	Eurotiomycetes
	A9	XP_746534.1	78-572	<i>Aspergillus fumigatus</i>	Eurotiales	Eurotiomycetes
	A10	XP_682472.1	83-577	<i>Aspergillus nidulans</i>	Eurotiales	Eurotiomycetes
	A11	XP_001590621.1	72-564	<i>Sclerotinia sclerotiorum</i>	Helotiales	Leotiomycetes
	A12	XP_001393409.1	71-554	<i>Aspergillus niger</i>	Eurotiales	Eurotiomycetes
	A13	XP_001594065.1	74-553	<i>Sclerotinia sclerotiorum</i>	Helotiales	Leotiomycetes
	A14	XP_023094139.1	13-419	<i>Aspergillus oryzae</i>	Eurotiales	Eurotiomycetes
	A15	XP_001394358.1	75-561	<i>Aspergillus niger</i>	Eurotiales	Eurotiomycetes
	A16	XP_009651693.1	90-471	<i>Verticillium dahliae</i>	Glomerellales	Sordariomycetes
	A17	XP_748839.1	77-548	<i>Aspergillus fumigatus</i>	Eurotiales	Eurotiomycetes
	A18	XP_001401809.1	78-549	<i>Aspergillus niger</i>	Eurotiales	Eurotiomycetes
	A19	XP_001393089.1	76-567	<i>Aspergillus niger</i>	Eurotiales	Eurotiomycetes
	A20	XP_001390411.1	73-547	<i>Aspergillus niger</i>	Eurotiales	Eurotiomycetes
	A21	XP_001398312.1	74-556	<i>Aspergillus niger</i>	Eurotiales	Eurotiomycetes
	A22	XP_001820636.1	76-549	<i>Aspergillus oryzae</i>	Eurotiales	Eurotiomycetes
	A23	XP_001399173.1	75-559	<i>Aspergillus niger</i>	Eurotiales	Eurotiomycetes
B	B1	XP_009650693.1	80-535	<i>Verticillium dahliae</i>	Glomerellales	Sordariomycetes
	B2	XP_018238457.1	70-528	<i>Fusarium oxysporum</i>	Hypocreales	Sordariomycetes
	B3	XP_011325880.1	1-344	<i>Fusarium graminearum</i>	Hypocreales	Sordariomycetes
	B4	XP_009656555.1	59-489	<i>Verticillium dahliae</i>	Glomerellales	Sordariomycetes
	B5	XP_680482.1	65-527	<i>Aspergillus nidulans</i>	Eurotiales	Eurotiomycetes
	B6	XP_001398581.2	67-508	<i>Aspergillus niger</i>	Eurotiales	Eurotiomycetes
	B7	XP_003851933.1	3-225	<i>Zymoseptoria tritici</i>	Capnodiales	Dothideomycetes
	B8	XP_001389566.2	173-616	<i>Aspergillus niger</i>	Eurotiales	Eurotiomycetes
	B9	XP_682533.1	53-202	<i>Aspergillus nidulans</i>	Eurotiales	Eurotiomycetes
	B10	XP_001822863.1	70-523	<i>Aspergillus oryzae</i>	Eurotiales	Eurotiomycetes
	B11	XP_001821143.3	76-525	<i>Aspergillus oryzae</i>	Eurotiales	Eurotiomycetes
	B12	XP_001394129.1	84-534	<i>Aspergillus niger</i>	Eurotiales	Eurotiomycetes
	B13	XP_018252729.1	73-523	<i>Fusarium oxysporum</i>	Hypocreales	Sordariomycetes
	B14	XP_011325853.1	24-327	<i>Fusarium graminearum</i>	Hypocreales	Sordariomycetes
	B15	XP_018383512.1	76-521	<i>Alternaria alternata</i>	Pleosporales	Dothideomycetes
	B16	XP_018243068.1	84-192	<i>Fusarium oxysporum</i>	Hypocreales	Sordariomycetes
	B17	XP_001589546.1	20-480	<i>Sclerotinia sclerotiorum</i>	Helotiales	Leotiomycetes
	B18	XP_008095378.1	74-535	<i>Colletotrichum graminicola</i>	Glomerellales	Sordariomycetes

Major Clades	Leaf labels	Protein IDs	Domain Position	Species	Order	Class
	B19	XP_003848450.1	75-555	<i>Zymoseptoria tritici</i>	Capnodiales	Dothideomycetes
	B20	XP_009221910.1	66-535	<i>Gaeumannomyces tritici</i>	Magnaporthales	Sordariomycetes
	B21	KLU85090.1	67-544	<i>Magnaporthiopsis poae</i>	Magnaporthales	Sordariomycetes
	B22	XP_018388182.1	79-539	<i>Alternaria alternata</i>	Pleosporales	Dothideomycetes
	B23	XP_661644.1	71-510	<i>Aspergillus nidulans</i>	Eurotiales	Eurotiomycetes
	B24	XP_018382797.1	60-529	<i>Alternaria alternata</i>	Pleosporales	Dothideomycetes
	B25	XP_018248758.1	54-507	<i>Fusarium oxysporum</i>	Hypocreales	Sordariomycetes
	B26	XP_011323064.1	61-517	<i>Fusarium graminearum</i>	Hypocreales	Sordariomycetes
	B27	XP_008096893.1	55-507	<i>Colletotrichum graminicola</i>	Glomerellales	Sordariomycetes
	B28	XP_008095122.1	90-557	<i>Colletotrichum graminicola</i>	Glomerellales	Sordariomycetes
	B29	XP_018258841.1	72-523	<i>Fusarium oxysporum</i>	Hypocreales	Sordariomycetes
	B30	XP_018258492.1	8-456	<i>Fusarium oxysporum</i>	Hypocreales	Sordariomycetes
	B31	XP_748245.1	59-504	<i>Aspergillus fumigatus</i>	Eurotiales	Eurotiomycetes
	B32	XP_001821840.1	55-502	<i>Aspergillus oryzae</i>	Eurotiales	Eurotiomycetes
	B33	XP_680663.1	143-283	<i>Aspergillus nidulans</i>	Eurotiales	Eurotiomycetes
	B34	XP_001402482.1	56-507	<i>Aspergillus niger</i>	Eurotiales	Eurotiomycetes
	B35	XP_009222743.1	57-538	<i>Gaeumannomyces tritici</i>	Magnaporthales	Sordariomycetes
	B36	KLU92702.1	57-538	<i>Magnaporthiopsis poae</i>	Magnaporthales	Sordariomycetes
	B37	XP_009228275.1	56-500	<i>Gaeumannomyces tritici</i>	Magnaporthales	Sordariomycetes
	B38	KLU92663.1	56-518	<i>Magnaporthiopsis poae</i>	Magnaporthales	Sordariomycetes
	B39	XP_029745326.1	96-566	<i>Pyricularia pennisetigena</i>	Magnaporthales	Sordariomycetes
	B40	XP_030979651.1	95-565	<i>Magnaporthe grisea</i>	Magnaporthales	Sordariomycetes
	B41	XP_003721410.1	95-565	<i>Magnaporthe oryzae</i>	Magnaporthales	Sordariomycetes
C	C1	XP_011322539.1	67-530	<i>Fusarium graminearum</i>	Hypocreales	Sordariomycetes
	C2	XP_003717620.1	71-526	<i>Magnaporthe oryzae</i>	Magnaporthales	Sordariomycetes
	C3	XP_030977148.1	70-517	<i>Magnaporthe grisea</i>	Magnaporthales	Sordariomycetes
	C4	XP_029744273.1	81-523	<i>Pyricularia pennisetigena</i>	Magnaporthales	Sordariomycetes
	C5	XP_008089135.1	144-523	<i>Colletotrichum graminicola</i>	Glomerellales	Sordariomycetes
	C6	KUI64534.1	64-513	<i>Valsa mali</i>	Diaporthales	Sordariomycetes
	C7	XP_023093874.1	89-514	<i>Aspergillus oryzae</i>	Eurotiales	Eurotiomycetes
	C8	XP_018379986.1	69-512	<i>Alternaria alternata</i>	Pleosporales	Dothideomycetes
D	D1	XP_008098422.1	76-518	<i>Colletotrichum graminicola</i>	Glomerellales	Sordariomycetes
	D2	XP_003856522.1	65-528	<i>Zymoseptoria tritici</i>	Capnodiales	Dothideomycetes
	D3	XP_681383.1	181-283	<i>Aspergillus nidulans</i>	Eurotiales	Eurotiomycetes
	D4	XP_023094235.1	67-515	<i>Aspergillus oryzae</i>	Eurotiales	Eurotiomycetes
	D5	XP_001401646.2	66-516	<i>Aspergillus niger</i>	Eurotiales	Eurotiomycetes
	D6	XP_001389907.2	72-510	<i>Aspergillus niger</i>	Eurotiales	Eurotiomycetes
	D7	XP_001395532.2	103-552	<i>Aspergillus niger</i>	Eurotiales	Eurotiomycetes
	D8	XP_001393845.1	90-532	<i>Aspergillus niger</i>	Eurotiales	Eurotiomycetes
	D9	XP_001397058.1	82-542	<i>Aspergillus niger</i>	Eurotiales	Eurotiomycetes
	D10	XP_001396750.2	144-576	<i>Aspergillus niger</i>	Eurotiales	Eurotiomycetes

Major Clades	Leaf labels	Protein IDs	Domain Position	Species	Order	Class
	D11	XP_001392929.2	91-544	<i>Aspergillus niger</i>	Eurotiales	Eurotiomycetes
E	E1	XP_009221918.1	74-536	<i>Gaeumannomyces tritici</i>	Magnaporthales	Sordariomycetes
	E2	KLU85094.1	73-459	<i>Magnaporthiopsis poae</i>	Magnaporthales	Sordariomycetes
	E3	XP_029746633.1	89-541	<i>Pyricularia pennisetigena</i>	Magnaporthales	Sordariomycetes
	E4	XP_030986500.1	89-541	<i>Magnaporthe grisea</i>	Magnaporthales	Sordariomycetes
	E5	XP_003716419.1	89-541	<i>Magnaporthe oryzae</i>	Magnaporthales	Sordariomycetes
	E6	XP_009226715.1	95-608	<i>Gaeumannomyces tritici</i>	Magnaporthales	Sordariomycetes
	E7	KLU81119.1	164-674	<i>Magnaporthiopsis poae</i>	Magnaporthales	Sordariomycetes
	E8	XP_958973.1	108-564	<i>Neurospora crassa</i>	Sordariales	Sordariomycetes
	E9	XP_029748856.1	204-661	<i>Pyricularia pennisetigena</i>	Magnaporthales	Sordariomycetes
	E10	XP_030983122.1	204-660	<i>Magnaporthe grisea</i>	Magnaporthales	Sordariomycetes
	E11	XP_003709031.1	199-648	<i>Magnaporthe oryzae</i>	Magnaporthales	Sordariomycetes
	E12	XP_009229246.1	72-554	<i>Gaeumannomyces tritici</i>	Magnaporthales	Sordariomycetes
	E13	KLU89793.1	18-485	<i>Magnaporthiopsis poae</i>	Magnaporthales	Sordariomycetes
	E14	XP_030980741.1	111-582	<i>Magnaporthe grisea</i>	Magnaporthales	Sordariomycetes
	E15	XP_003710469.1	96-531	<i>Magnaporthe oryzae</i>	Magnaporthales	Sordariomycetes
	E16	XP_009227107.1	93-235	<i>Gaeumannomyces tritici</i>	Magnaporthales	Sordariomycetes
	E17	KLU81081.1	150-657	<i>Magnaporthiopsis poae</i>	Magnaporthales	Sordariomycetes
	E18	XP_009222105.1	143-622	<i>Gaeumannomyces tritici</i>	Magnaporthales	Sordariomycetes
	E19	XP_030982425.1	148-619	<i>Magnaporthe grisea</i>	Magnaporthales	Sordariomycetes
	E20	XP_029748802.1	154-620	<i>Pyricularia pennisetigena</i>	Magnaporthales	Sordariomycetes
	E21	XP_003710210.1	148-616	<i>Magnaporthe oryzae</i>	Magnaporthales	Sordariomycetes
F	F1	XP_018250559.1	71-532	<i>Fusarium oxysporum</i>	Hypocreales	Sordariomycetes
	F2	XP_011322804.1	74-532	<i>Fusarium graminearum</i>	Hypocreales	Sordariomycetes
	F3	XP_009216387.1	79-558	<i>Gaeumannomyces tritici</i>	Magnaporthales	Sordariomycetes
	F4	XP_030982200.1	87-564	<i>Magnaporthe grisea</i>	Magnaporthales	Sordariomycetes
	F5	XP_029748473.1	83-560	<i>Pyricularia pennisetigena</i>	Magnaporthales	Sordariomycetes
G	G1	XP_003850170.1	77-524	<i>Zymoseptoria tritici</i>	Capnodiales	Dothideomycetes
	G2	XP_023091640.1	75-518	<i>Aspergillus oryzae</i>	Eurotiales	Eurotiomycetes
	G3	XP_018388746.1	76-527	<i>Alternaria alternata</i>	Pleosporales	Dothideomycetes
	G4	XP_008096050.1	3-73	<i>Colletotrichum graminicola</i>	Glomerellales	Sordariomycetes
	G5	XP_029750270.1	78-530	<i>Pyricularia pennisetigena</i>	Magnaporthales	Sordariomycetes
	G6	XP_030980784.1	78-530	<i>Magnaporthe grisea</i>	Magnaporthales	Sordariomycetes
	G7	XP_003720204.1	78-530	<i>Magnaporthe oryzae</i>	Magnaporthales	Sordariomycetes
	G8	XP_009225032.1	64-488	<i>Gaeumannomyces tritici</i>	Magnaporthales	Sordariomycetes
	G9	KLU85867.1	62-500	<i>Magnaporthiopsis poae</i>	Magnaporthales	Sordariomycetes
	G10	XP_009655052.1	24-300	<i>Verticillium dahliae</i>	Glomerellales	Sordariomycetes
	G11	XP_018248766.1	81-531	<i>Fusarium oxysporum</i>	Hypocreales	Sordariomycetes
	G12	XP_011318013.1	194-561	<i>Fusarium graminearum</i>	Hypocreales	Sordariomycetes
H	H1	XP_003852884.1	71-535	<i>Zymoseptoria tritici</i>	Capnodiales	Dothideomycetes
	H2	XP_659376.1	76-527	<i>Aspergillus nidulans</i>	Eurotiales	Eurotiomycetes

Major Clades	Leaf labels	Protein IDs	Domain Position	Species	Order	Class
	H3	XP_001819091.1	75-526	<i>Aspergillus oryzae</i>	Eurotiales	Eurotiomycetes
	H4	XP_750792.1	74-526	<i>Aspergillus fumigatus</i>	Eurotiales	Eurotiomycetes
	H5	XP_001396085.1	72-521	<i>Aspergillus niger</i>	Eurotiales	Eurotiomycetes
	H6	XP_731510.1	78-528	<i>Aspergillus fumigatus</i>	Eurotiales	Eurotiomycetes
	H7	XP_001818628.3	90-540	<i>Aspergillus oryzae</i>	Eurotiales	Eurotiomycetes
I	I1	XP_018385975.1	88-504	<i>Alternaria alternata</i>	Pleosporales	Dothideomycetes
	I2	XP_008098258.1	78-423	<i>Colletotrichum graminicola</i>	Glomerellales	Sordariomycetes
	I3	XP_009656412.1	80-476	<i>Verticillium dahliae</i>	Glomerellales	Sordariomycetes
	I4	XP_008098257.1	1-109	<i>Colletotrichum graminicola</i>	Glomerellales	Sordariomycetes
	I5	XP_003847726.1	77-532	<i>Zymoseptoria tritici</i>	Capnodiales	Dothideomycetes
	I6	XP_009226702.1	87-535	<i>Gaeumannomyces tritici</i>	Magnaporthales	Sordariomycetes
	I7	XP_030981492.1	91-546	<i>Magnaporthe grisea</i>	Magnaporthales	Sordariomycetes
	I8	XP_029749282.1	89-542	<i>Pyricularia pennisetigena</i>	Magnaporthales	Sordariomycetes
	I9	XP_003720117.1	90-543	<i>Magnaporthe oryzae</i>	Magnaporthales	Sordariomycetes
	I10	XP_018386857.1	85-536	<i>Alternaria alternata</i>	Pleosporales	Dothideomycetes
	I11	KUI70248.1	86-505	<i>Valsa mali</i>	Diaporthales	Sordariomycetes
	I12	XP_008093627.1	40-412	<i>Colletotrichum graminicola</i>	Glomerellales	Sordariomycetes
	I13	XP_009652609.1	77-488	<i>Verticillium dahliae</i>	Glomerellales	Sordariomycetes
	I14	XP_008091349.1	79-521	<i>Colletotrichum graminicola</i>	Glomerellales	Sordariomycetes
	I15	XP_018250707.1	104-554	<i>Fusarium oxysporum</i>	Hypocreales	Sordariomycetes
	I16	XP_011322847.1	77-527	<i>Fusarium graminearum</i>	Hypocreales	Sordariomycetes
	I17	XP_009225346.1	75-527	<i>Gaeumannomyces tritici</i>	Magnaporthales	Sordariomycetes
	I18	KLU84443.1	82-488	<i>Magnaportheopsis poae</i>	Magnaporthales	Sordariomycetes
	I19	XP_029749156.1	75-535	<i>Pyricularia pennisetigena</i>	Magnaporthales	Sordariomycetes
	I20	XP_030981117.1	106-560	<i>Magnaporthe grisea</i>	Magnaporthales	Sordariomycetes
	I21	XP_003719248.1	106-560	<i>Magnaporthe oryzae</i>	Magnaporthales	Sordariomycetes

Table 3.1.3: List of Fae protein IDs from 18 fungal species, representing each leaf of the phylogenetic tree in Fig. 3.1.3., grouped into 9 major clades. The number-range in the 'domain position' column indicate the amino acid position predicted to contain tannase domain in each Fae protein sequence.

Furthermore, a phylogenetic analysis using MEGA tool was performed, of combined as well as individual Fae sequences from host-specific *M. oryzae* strains, isolated from various cereal crops such as rice, wheat and millet, and *M. grisea* as an outgroup (Fig. 3.1.4 and Fig. 3.1.5). Interestingly, this analysis showed that three *M. oryzae* Fae sequences, namely MGG_09404, MGG_09732 and MGG_08737, diverged likely in a host-specific manner (Fig. 3.1.5).

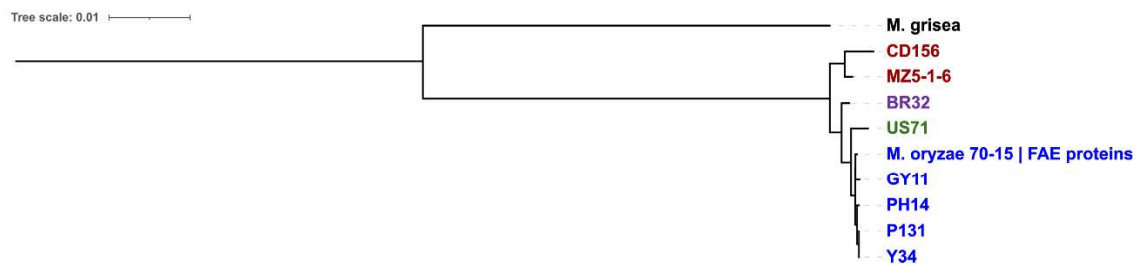


Figure 3.1.4. Phylogenetic tree depicting combined analysis of Fae sequences in host-specific *M. oryzae* isolates from rice (*Oryza*; blue), wheat (*Triticum*; violet), foxtail millet (*Setaria*; green) and finger millet (*Eleusine*; red), with *M. grisea* (black) as an outgroup.

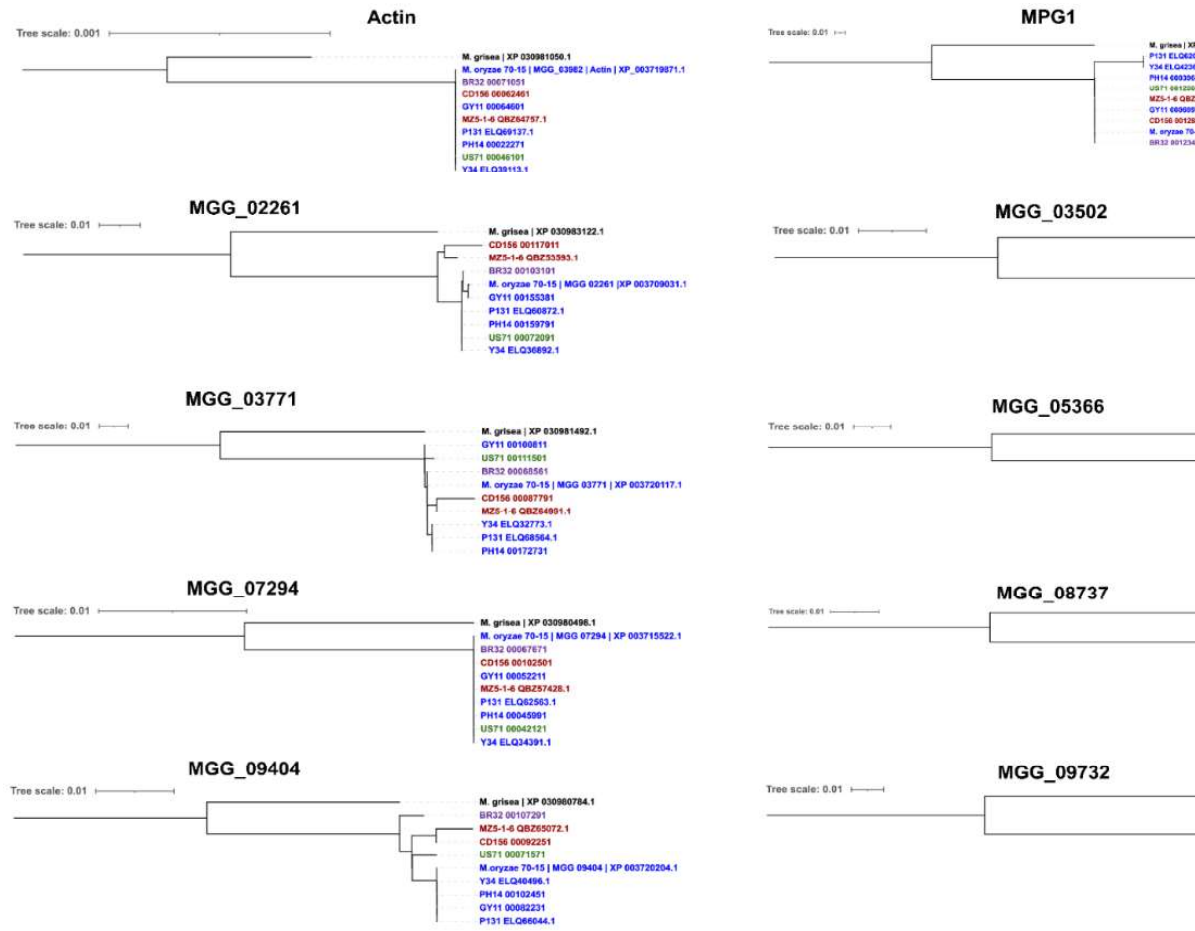
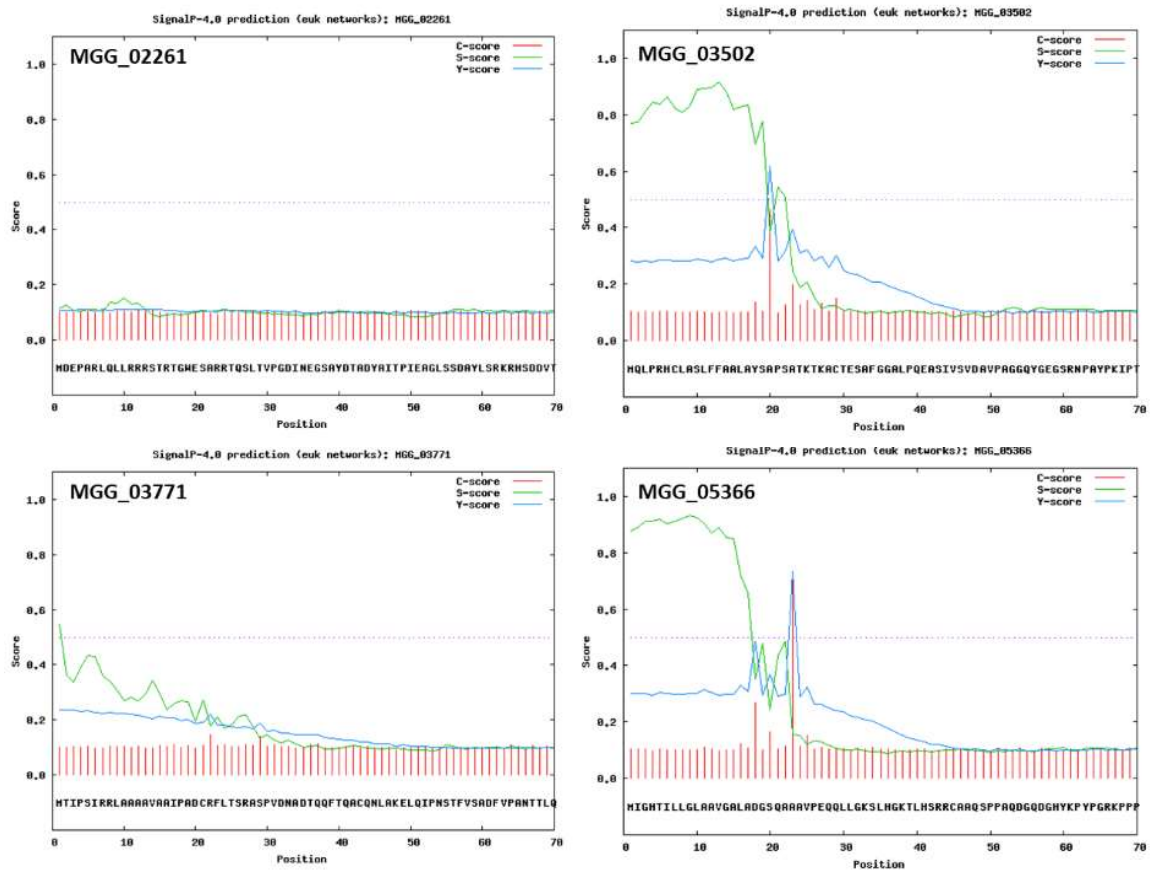


Figure 3.1.5. Phylogenetic trees depicting analysis of individual Fae sequences from host-specific ... trees for actin and Mpg1 (fungal hydrophobin), from host-specific *M. oryzae* isolates, were generated as a co-specific divergence in these presumably conserved proteins. Host-specific *M. oryzae* isolates from rice (*Oryza sativa*; blue), foxtail millet (*Setaria*; green) and finger millet (*Eleusine*; red), with *M. grisea* (black) as an outgroup, were used.

3.1.4 Prediction of conventional signal peptide in Fae by SignalP tool

CWDEs including Fae, generally would function outside the cell, hence the secretory nature of Fae in *M. oryzae* was studied. To begin with, the presence or absence of a conventional secretory signal peptide in the nine Fae was checked *in silico* using SignalP program. This analysis showed a likely presence of the conventional secretory signal peptide in seven out of nine Fae in *M. oryzae* (Fig. 3.1.6). Position of the secretory signal peptide and location of its possible cleavage site for each given Fae sequence is shown in Table 3.1.4.



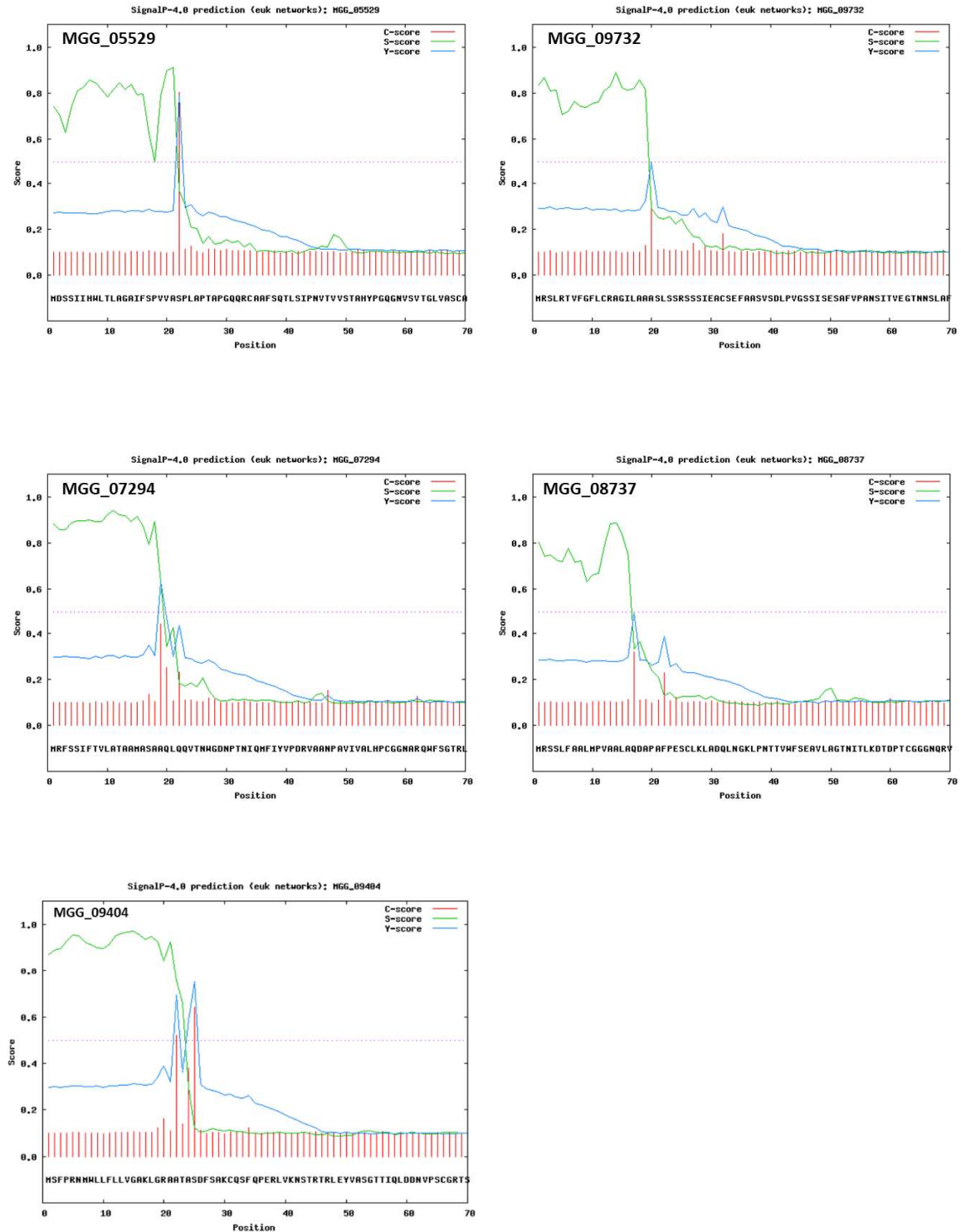


Figure 3.1.6. Prediction of signal peptide by SignalP tool. The figure shows the output file obtained upon executing the SignalP web-program for individual Fae protein sequences. A horizontal dotted line denotes the default threshold score and a signal above which would be predicted to contain a signal peptide for a given protein sequence.

Gene ID	Signal Peptide	
	<i>Position</i>	<i>Cleavage site</i>
MGG_07294.6	1 – 18	Between 18 and 19 aa
MGG_08737.6	1 – 16	Between 16 and 17 aa
MGG_03771.6	–	None
MGG_09404.6	1 – 24	Between 24 and 25 aa
MGG_05529.6	1 – 21	Between 21 and 22 aa
MGG_03502.6	1 – 19	Between 19 and 20 aa
MGG_05366.6	1 – 22	Between 22 and 23 aa
MGG_02261.6	–	None
MGG_09732.6	1 – 19	Between 19 and 20 aa

Table 3.1.4: Amino acid positions of the predicted signal peptide and its cleavage site in individual Fae sequences in *M. oryzae*.

3.1.5 Validation of two *FAEs* for the presence of signal peptide by Yeast Secretion Trap (YST)-approach

Further, to validate this observation, two putative *FAE* genes (Gene ID: MGG_05229 and MGG_07294), that showed presence of a secretory signal peptide by *in silico* analysis, were randomly selected and subjected to YST system as described earlier (Chapter 2). Here, pYST2 vector, containing *SUC2* invertase gene devoid of a native signal peptide was used. The ORFs of MGG_05529 and MGG_07294 were PCR-amplified from *M. oryzae* WT genomic DNA, using the primer pairs: MGG_05529 (Forward: 5'-ATGGA CTCTGTCAATCATTCACTGG-3' and Reverse: 5'-CCCATTCCACTTTGACCTG-3') & MGG_07294 (Forward: 5'-ATGCGTTTCTCCAGCATCTTC-3' and Reverse: 5'-CGCAATGAGACCAAAGAACC-3'). Individual PCR products were then cloned in-frame, upstream to the *SUC2* gene in pYST2 vector by blunt-end ligation at *NotI* site after end-filling, followed by *E. coli* DH5 α

transformation. The *E. coli* transformants obtained on Luria-agar plates containing 100 µg/mL ampicillin antibiotic were screened by relevant RE digestion (Fig. 3.1.7), and those with the desired restriction digestion pattern were confirmed by DNA sequencing. The resulting plasmids, denoted as pYST2-5529 and pYST2-7294, were then individually introduced into budding yeast (*S. cerevisiae*) DBYα2445 strain which does not carry its native *SUC2* invertase gene. Yeast transformants, thus obtained, were confirmed for the presence of the cloned ORF sequence by relevant colony PCR (Fig. 3.1.7). Next, these yeast transformants were allowed to grow on selection medium containing sucrose as the sole carbon source. Thus, neither the untransformed yeast nor that transformed with only a backbone-vector (pYST2) would be able to grow on this selection medium. However, a yeast transformant expressing the Suc2 fused with Fae, presumably containing a secretory signal peptide, would facilitate the secretion of Suc2-invertase and utilize sucrose in the selection medium. Importantly, the yeast transformants harbouring the plasmid with Suc2 fused to either of the two *FAE* genes grew on sucrose agar medium, confirming the presence of a signal peptide and thereby confirming the secretory nature of the Fae encoded by genes MGG_05529 and MGG_07294 (Fig. 3.1.7). Altogether, the *in silico* analysis and the YST-based assay indicate that majority of the Fae enzymes are secreted by *M. oryzae*.

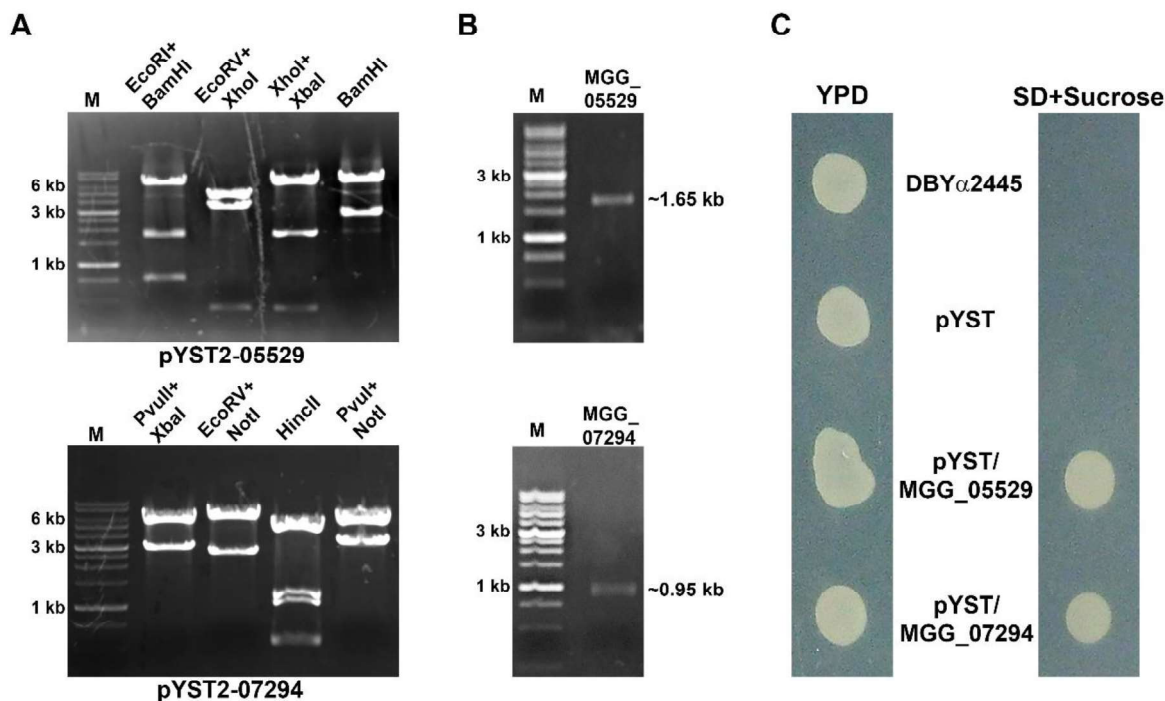
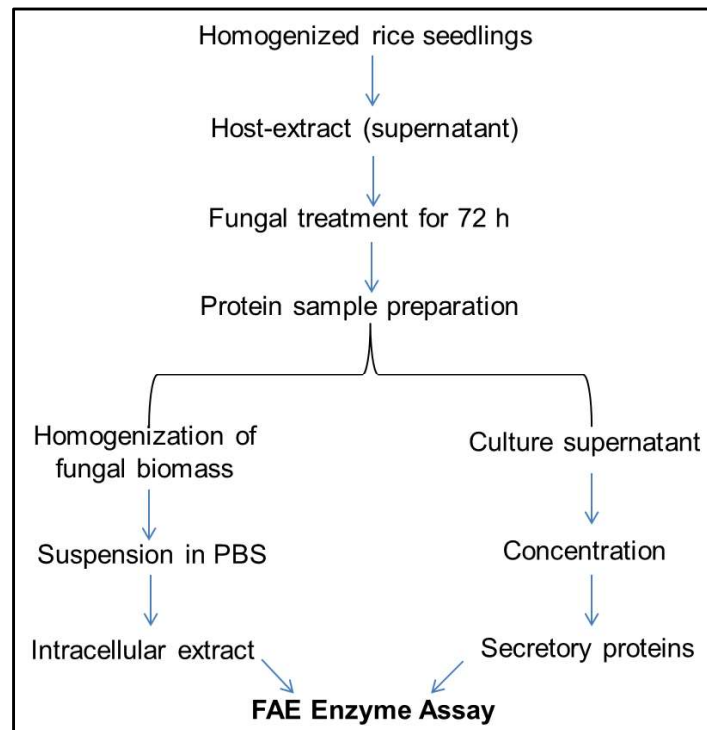


Figure 3.1.7. *M. oryzae* feruloyl esterases are secretory in nature. (A) Confirmation of pYST2-05529 and pYST2-07294 by RE digestion. Expected band-sizes obtained upon digestion with different restriction enzymes: pYST2-05529– *EcoRI*+*BamHI*–~7, 1.5, 0.8 kb; *EcoRV*+*XhoI*–~5.5, 3.3, 0.4 kb; *XhoI*+*XbaI*–~7, 1.7, 0.4 kb; *BamHI*–~7, 2.3 kb and pYST2-05529– *PvuII*+*XbaI*–~5.6, 3 kb; *EcoRV*+*NotI*–~5.8, 2.7 kb; *HincII*–~4.7, 1.2, 1, 0.5 kb; *PvuI*+*NotI*–~5.5, 3 kb. (B) Confirmation of yeast transformants by colony-PCR using gene-specific primers for the presence of respective recombinant plasmids. Numbers on right-hand side indicate the expected size of the PCR-product. Numbers on the left-hand side, in both (A) and (B), denote representative sizes of the DNA fragments in the marker (M). (C) The Yeast Secretion Trap based assay depicting growth of the transformants expressing *M. oryzae* FAE (MGG_05529 or MGG_07294) when compared to the no-growth, on SD + Sucrose, of the recipient strain (DBY α 2445) with or without the backbone vector (pYST).

3.1.6 Effect of host leaf-extract on fungal Fae activity

In order to check the effect of host leaf-extract on Fae enzyme activity, 3-day-old vegetative culture of WT *M. oryzae* grown in liquid YEG medium, with or without crude rice leaf extract, was used. Protein samples were prepared from fungal biomass (intracellular proteins) and culture supernatant (secretory proteins), essentially as described earlier (Kachroo et al., 1997), followed by biochemical spectrophotometric enzyme assay using

Fae-specific substrate, 4-nitrophenyl ferulate (Institute of Chemistry, Slovak Academy of Sciences, Bratislava), as described previously (Mastihuba et al., 2002). Protein estimation was carried out using Bradford reagent and standard curve method (B6916; Sigma-aldrich, USA). Finally, specific activity (mU mg^{-1}) of Fae was calculated, based on standard curve of 4-nitrophenol (Fig. 3.1.8A), for intracellular and secretory protein fractions from both control and rice-extract-treated samples. Overall process is summarized in the following flow-chart:



Here, the total Fae enzyme activity was found to be significantly higher ($166 \pm 3.33 \text{ mU mg}^{-1}$; $P < 0.001$, Table 3.1.5) in the extracellular (secretory) fraction of the culture grown in the presence of rice leaf extract, when compared with that ($29 \pm 0.69 \text{ mU mg}^{-1}$, Table 3.1.5) without the host extract (Fig. 3.1.8B). Importantly, the total enzyme activity in the intracellular fraction was less and remained largely unchanged irrespective of the presence or absence of the host leaf extract (Fig. 3.1.8B). These results show that most *M. oryzae* Fae

are secretory and that their expression is induced by the host-derived factors, suggesting a likely role for the CWDE in blast fungal pathogenesis.

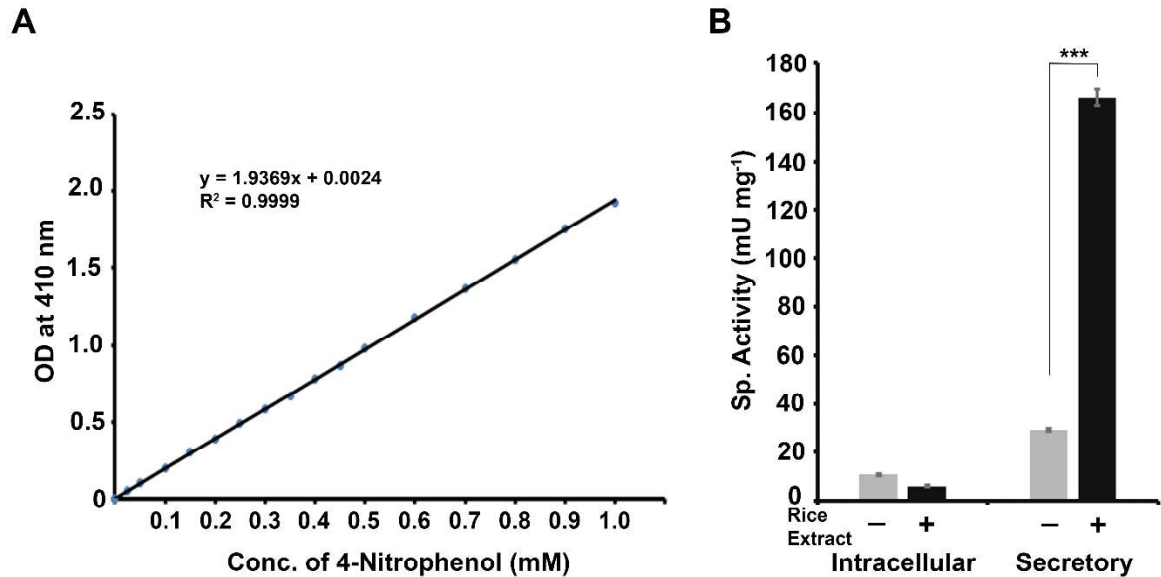


Figure 3.1.8. *M. oryzae* feruloyl esterases are induced by host leaf extract. (A) Standard curve of 4-nitrophenol (4-NP), showing OD values at 410 nm for known concentrations of 4-NP ranging from 0.025–1.0 mM. **(B)** A bar chart showing Fae enzyme activity in the intracellular versus extracellular (secretory) fraction of the *M. oryzae* culture grown in the presence or absence of rice leaf extract. The data is represented as mean ± s.d.m. from three independent experiments. ***, $P < 0.001$.

Sample		Sp. Enzyme Activity (mU mg ⁻¹)			Mean Sp. Enzyme Activity (mU mg ⁻¹)	Fold change (treated/untreated)
Untreated	Intracellular	10.51	10.35	11.12	10.66 ± 0.41	-
Treated		5.35	6.10	6.40	5.95 ± 0.54	0.56
Untreated	Secretory	28.20	29.40	29.44	29.01 ± 0.69	-
Treated		162.35	167.53	168.57	166.15 ± 3.33	5.73

Table 3.1.5: Fae-enzyme activity assay. Values showing Fae-specific enzyme activity (mU mg⁻¹) in different samples mentioned. Activity assay was performed independently for three times and the data is represented as mean values ± s.d.m. Fold-change was calculated by taking a ratio of mean sp. activity corresponding to treated and untreated samples for both intracellular and secretory fractions. Significant change in sp. activity is highlighted in grey-shaded cell.

3.1.7 Gene expression profiling of *FAEs* during pathogenic development in *M. oryzae* by qRT-PCR

3.1.7.1 Gene expression analysis under host- or pathogenicity-mimic conditions

CWDEs are generally expressed under tight transcriptional regulation (Zheng et al., 2009). Given that *M. oryzae* Fae secretion was induced in the presence of rice leaf extract, possibly by the complex mixture of host factor(s) including the individual plant cell wall components. Therefore, the transcript levels of nine *FAEs* were studied in response to the individual host cell wall components and also pathogenicity-mimic conditions, as mentioned below in Table 3.1.6:

<u>Conditions / sole carbon source</u>	<u>Significance</u>
<i>N₂ starvation</i>	mimics nutrient stress condition during infection
<i>Cutin monomers</i>	promote appressorium formation
<i>Pectin</i>	component of plant cell-wall
<i>Xylan</i>	component of plant cell-wall
<i>Ferulic acid (FA)</i>	component released from polymers like pectin & xylan
<i>N-acetylglucosamine (NAG)</i>	amino sugar, basic unit of chitin (fungal cell wall)
<i>Glucose</i>	control

Table 3.1.6: List of different media conditions and their significance in *FAE* gene expression analysis.

First, the vegetative culture of WT *M. oryzae* was grown for 3 days in liquid complete medium (CM). Fungal biomass was then harvested and washed thrice with sterile distilled water followed by aseptic transfer in nearly equal amounts to the following seven different media conditions: 1) Minimal medium (MM) as a control condition, 2) MM (w/o glucose)

+ 0.03% cutin monomers (1,16-hexadecanediol; Sigma); 3) MM (w/o glucose) + 0.03% ferulic acid (Sigma); 4) MM minus NaNO₃ (nitrogen starvation); 5) MM (w/o glucose) + 1% pectin (Sigma); 6) MM (w/o glucose) + 1% N-acetylglucosamine (NAG; HiMedia) and 7) MM (w/o glucose) + 1% xylan (Sigma). Fungal cultures were then treated in aforementioned media conditions for 48 hours under shaking conditions at 28 °C, followed by total RNA isolation (Fig. 3.1.9A) and first-strand cDNA synthesis (Fig. 3.1.9B), using a procedure described in Chapter 2. Synthesized cDNA was then subjected to the optimized qRT-PCR analysis, as described earlier in Chapter 2. The primers for qRT-PCR analysis, listed in Table 3.1.7, were first confirmed for specificity by conventional PCR (Fig. 3.1.9C).

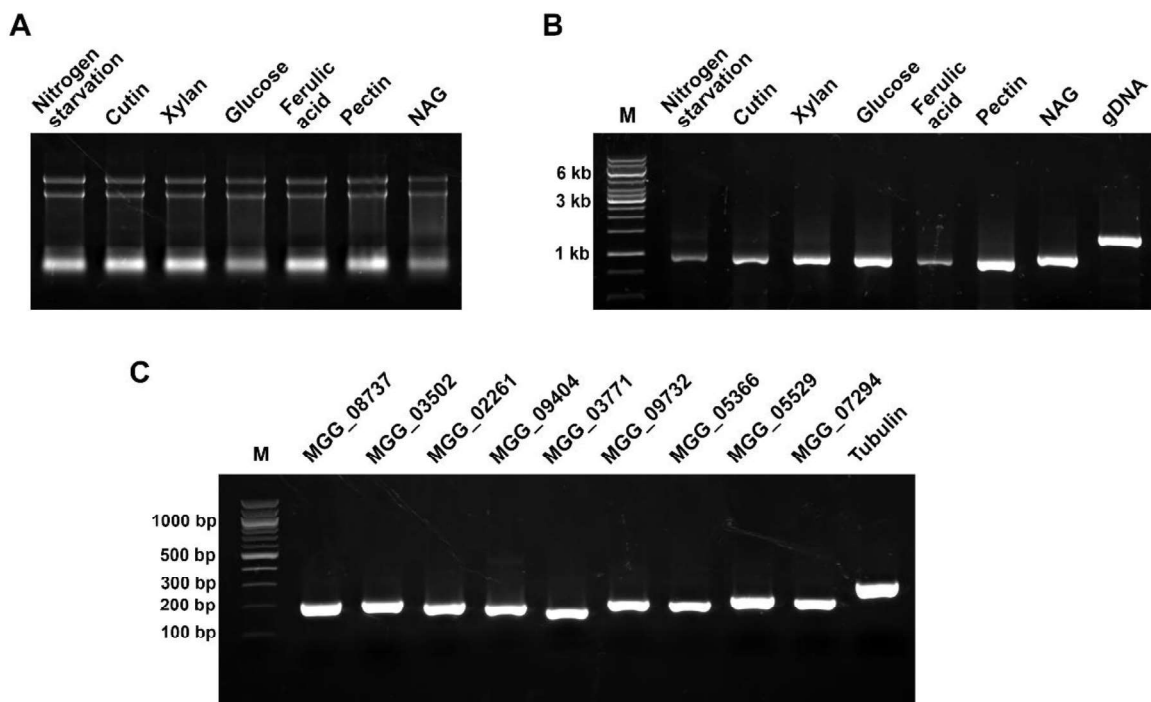


Figure 3.1.9. Analysis of total RNA, cDNA and primers' specificity for qRT-PCR. (A) 1% agarose gel showing characteristic rRNA bands in the total RNA indicating a good quality of RNA isolated from each samples mentioned. **(B)** PCR with each cDNA samples using β -tubulin primers. Amplification product showing a single-band of desired ~1 kb size, as compared to ~1.5 kb with genomic DNA (gDNA), confirms the successful first-strand cDNA synthesis. **(C)** PCR with qRT-PCR primers (Table 3.1.7) using gDNA as a template.

Single amplification products, in the range of ~200-250 bp size confirms specificity of the respective primer sequences. Numbers on the left-hand side, in both (B) and (C), denote representative sizes of the DNA fragments in the marker (M).

Primer	Sequence (5' → 3')
MGG_08737F	CACTCTTTGCGGCTCTGATG
MGG_08737R	GTCGTGACGAACATGGCAAC
MGG_03502F	CCAGGCATTGTCTCGCCTCG
MGG_03502R	ACAACCACAGCACACAGCTC
MGG_02261F	CTACGCCATCACACCCATCG
MGG_02261R	GACAAGGCGCTTGGCGAGC
MGG_09404F	GCGAAACTCGGTCGAGCAGC
MGG_09404R	CAGATGTTTACGTCCACGACC
MGG_03771F	GATTTCTGACCAGCAGGGCGTCT
MGG_03771R	GGGTCGACGTTGGGGAAGT
MGG_09732F	GAGGAGCCTAAGGACGGTTT
MGG_09732R	GGCTGTTGTTGGTGCCTTCT
MGG_05366F	GATAGGGCACACGATACTGC
MGG_05366R	AGCCTTATCCTGGCAGAAAGC
MGG_05529F	CATTCAGTGGTAAACGCTGGC
MGG_05529R	AAGCTGGTGCCGATGCTGTC
MGG_07294F	GCGTTTCTCCAGCATCTTCAC
MGG_07294R	GTGCCGCTGAACCATTGGCGT
MGG_00604F (β -TUB)	GAGTCCAACATGAACGATCT
MGG_00604R (β -TUB)	GTACTCCTCTTCTCCTCGT

Table 3.1.7: List of oligonucleotide primers used for qRT-PCR analysis of *FAE* gene expression.

Quantitative RT-PCR analysis showed that, although there was no obvious pattern in accumulation of any particular transcript, *FAE* genes did express differentially, with majority of them accumulating >1.5 fold higher in response to the plant cell wall components. While this observation is consistent with a previously reported similar upregulation of *FAEs* in *Aspergillus niger* (de Vries et al., 2002) and *Fusarium graminearum* (Balcerzak et al., 2012), it remains to be tested whether a combination of more than one host cell wall component would cause further upregulation in expression of any

particular *FAE* gene. Interestingly, majority of the *FAEs* showed a ≥ 2 -fold increase in expression in the presence of NAG (Fig. 3.1.10). Whereas, expression of almost all the *FAEs* was significantly lowered under N₂ starvation or in the presence of xylan (Fig. 3.1.10). These results suggest that the expression of *M. oryzae FAE* could be induced by likely the activity of plant and/or fungal chitinase during the host-pathogen interaction.

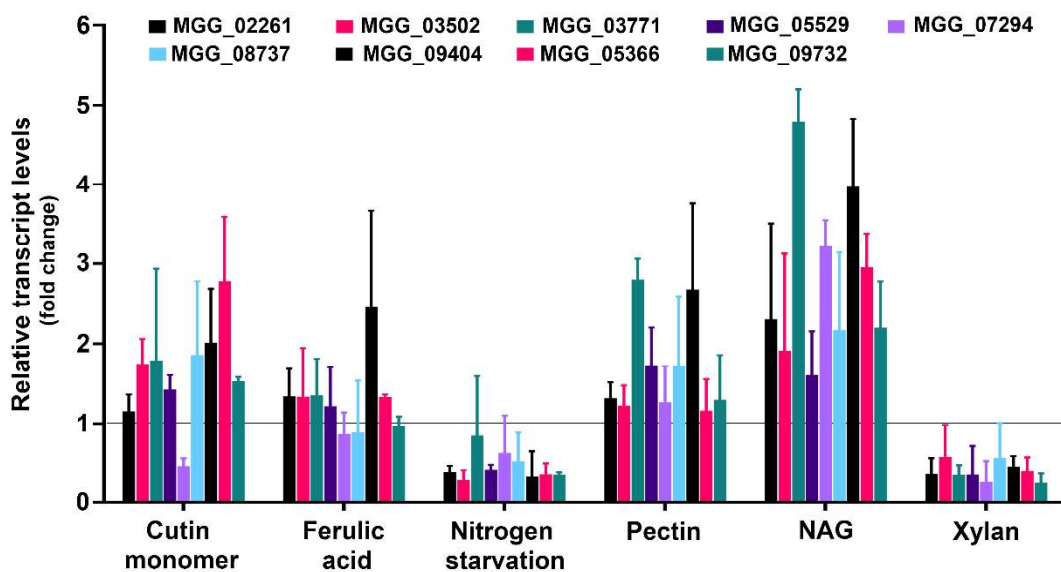
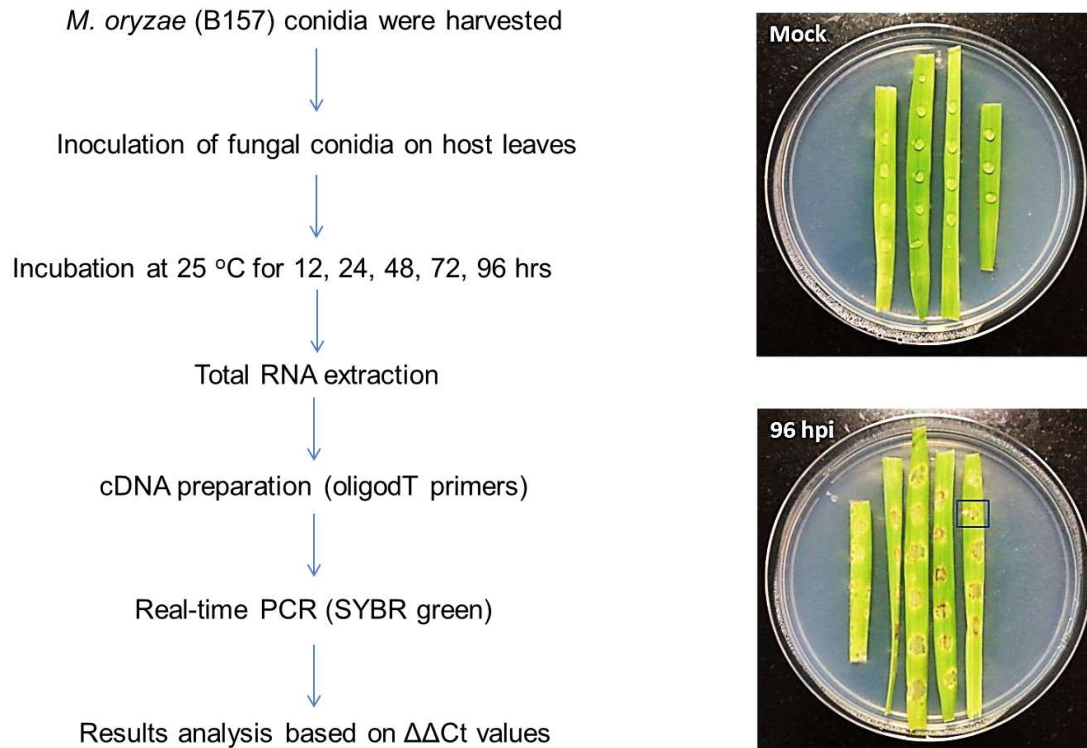


Figure 3.1.10. Differential expression of feruloyl esterase genes under different culture conditions. A bar chart showing relative transcript levels of nine *FAEs* in *M. oryzae* vegetative culture grown under different conditions. The cultures were grown in minimal medium with either 0.03% cutin monomers (1, 16 - hexadecanediol), 0.03% ferulic acid, nitrogen-starvation, 1% Pectin, 1% N-acetylglucosamine (NAG) or 1% Xylan, for 48 h before harvesting the biomass. The *FAE* transcript levels were estimated relative to those in the vegetative culture grown in minimal medium containing 1% glucose as a control condition. The horizontal line corresponding to the fold change 1 represents normalized transcript levels for the control condition. β -tubulin was used as an endogenous control. Data represents mean values \pm s.d.m. from three independent biological replicates with technical triplicates each time.

3.1.7.2 Gene expression analysis at different stages of pathogenic development

The expression of *FAEs* during different stages of infection (*in vivo*) was studied, using a method, with modifications, reported earlier (Skamnioti and Gurr, 2007). Briefly, a 15-20 μ L WT conidial suspension ($\sim 10^5$ conidia/mL; containing 0.05% gelatin) was drop-inoculated on the surface-sterilized 2–3-week-old barley leaf blades placed on to kinetin-agar plates, followed by incubation under dark (8 h) and light (14 h) cycles at 25 °C. Samples for RNA extraction were collected by excising inoculated portion of the leaf blades at different time-points viz. 12, 24, 48, 72- and 96-hours post inoculation (hpi). The selected time-points signify different stages of blast fungal infection cycle i.e., – pre-invasive appressorial development (12 h), host penetration and colonization (24-48 h) followed by necrotrophic growth phase (48-96 h). The process flow-chart is shown below along with a representative image of the experimental setup (plates on right-hand side).



Next, the total RNA was isolated (Fig. 3.1.11A) from the respective samples followed by first-strand cDNA synthesis (Fig. 3.1.11B), using a procedure described in Chapter 2.

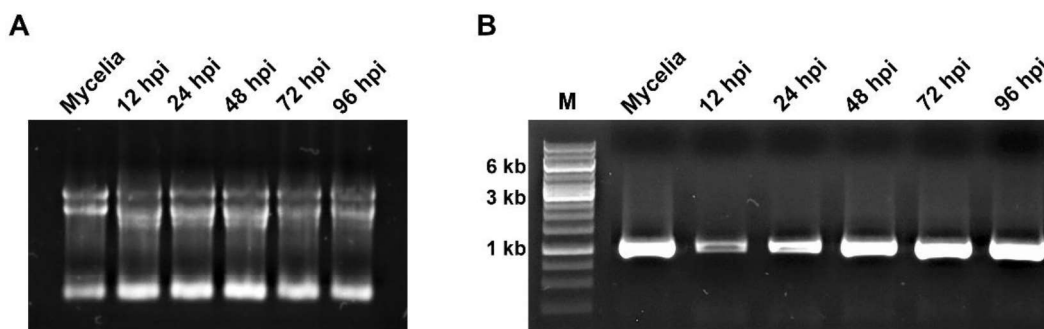


Figure 3.1.11. Analysis of RNA and cDNA samples for qRT-PCR. (A) 1% agarose gel showing characteristic rRNA bands in the total RNA isolated from each samples mentioned, indicating a good quality of RNA preparation. (B) PCR with each cDNA samples using β -tubulin primers. Amplification product showing a single-band of desired ~1 kb size confirms the successful first-strand cDNA synthesis. Numbers on the left-hand side denote representative sizes of the DNA fragments in the marker (M).

The relative transcript levels of all the nine *FAEs* were estimated by qRT-PCR during infection stages and compared with those from the vegetative mycelia grown in liquid complete medium. While, almost all the *FAE* genes showed differential upregulation at different phases of pathogenic life cycle, remarkably, MGG_08737, hereafter referred as *FAE1*, showed a significant increase in relative transcript levels (~300-fold) during pre-invasive appressorial development and host penetration stages (12 and 24 hpi) when compared to those of the other *FAEs* from the vegetative mycelia (Fig. 3.1.12). The *FAE1* transcript levels further increased (~470-fold) during the subsequent host colonization (48 hpi) and remained at elevated level (~293-fold) at 72 hpi, followed by a sharp decline (~27-fold) at 96 hpi (Fig. 3.1.12).

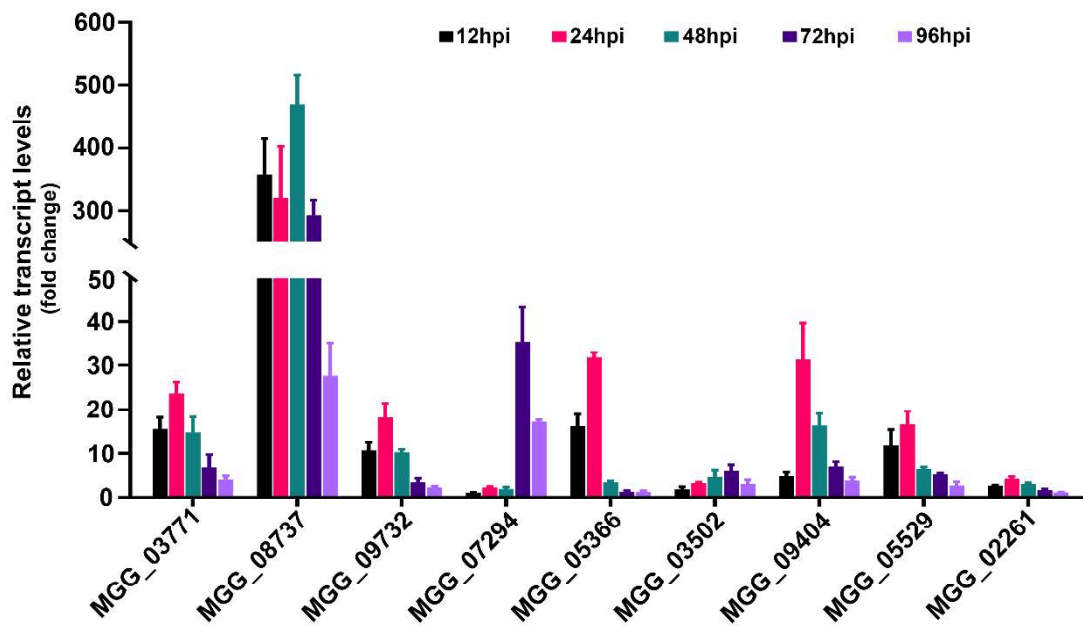


Figure 3.1.12. Differential expression of feruloyl esterase genes during pathogenesis in *M. oryzae*. A bar chart depicting relative transcript levels of nine *FAEs* during different stages of pathogenic development. Samples were harvested at the time points mentioned and the transcript levels were compared to those from vegetative mycelia grown in liquid CM as a control condition. β -tubulin was used as an endogenous control. A sample from mock-inoculation i.e., leaves inoculated with only 0.05% gelatin solution, was used as a negative control for any non-specific amplification during qRT-PCR. Data represents mean values \pm s.d.m. from three independent biological replicates with technical triplicates each time.

Importantly, the *FAEI* transcript profile here is in accordance with the global transcriptome reported earlier in *M. oryzae* (Jeon et al., 2020). This report showed that MGG_08737 (*FAEI*) significantly upregulates at 18 hpi (161-fold), 27 hpi (82-fold), 36 hpi (130-fold), 45 hpi (147-fold) and 72 hpi (228-fold) during infection cycle of *M. oryzae* (derived from Jeon et al., 2020). These observations indicate that feruloyl esterases, particularly Fae1, has an important role during pathogenesis in *M. oryzae*.

Section 3.2:

Investigating the role of a feruloyl esterase (Fae1) in pathogenesis of *M. oryzae*

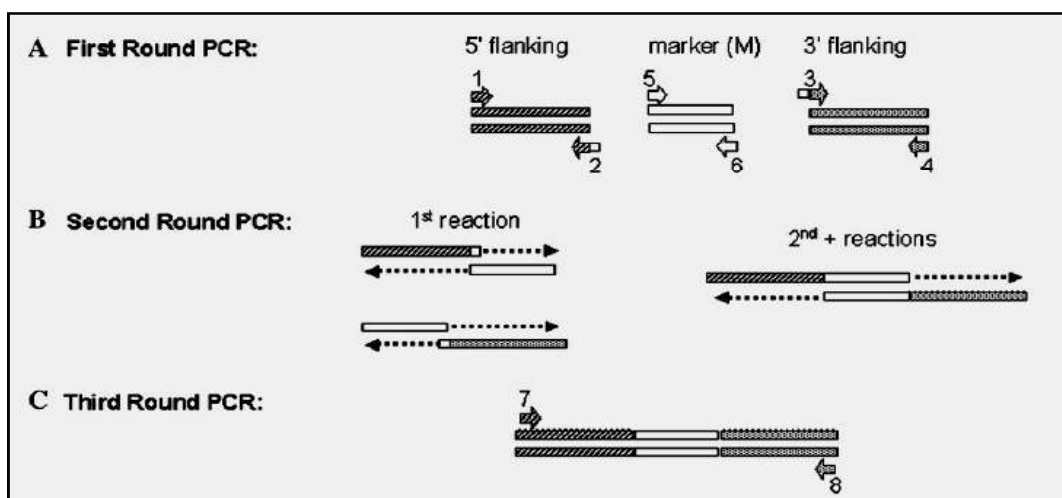
Section 3.2: Investigating the role of a feruloyl esterase (Fae1) in pathogenesis of *M. oryzae*

In microbial pathogens, feruloyl esterases (Fae) and other CWDEs often occur as gene families. As described earlier (section 3.1), *M. oryzae* consists of nine putative *FAEs*, majority of which showed upregulation during pre- and post-penetration stages of fungal infection cycle. Remarkably, expression profile of *FAE1* (MGG_08737) was striking among other *FAEs* in *M. oryzae*, during plant infection. It would be therefore interesting to study whether Fae1 plays any important role in pathogenesis of *M. oryzae*. This section focuses on the generation of a *FAE1*-deletion mutant of *M. oryzae*, followed by its molecular and phenotypic characterization, particularly with respect to pathogenic stages of the fungal infection cycle.

3.2.1 Generation of *FAE1*-deletion mutant (*fae1Δ*) of *M. oryzae*

3.2.1.1 Preparation of *FAE1*-deletion cassette and fungal transformation

FAE1 gene (Gene ID: MGG_08737) deletion cassette was made by double-joint PCR approach, involving three sequential rounds of PCR (Yu et al., 2004; Fig. 3.2.1).



(Adapted from Yu et al., 2004)

Figure 3.2.1. Schematic representation of double-joint PCR approach. (A) 5'- and 3'-flanking sequences amplified with respective primer pairs, wherein primer no. 2 and 3 consists of sequences, as shown by the white boxes, overlapping with that of the ends of the selectable marker (M). **(B)** Joining of the DNA fragments occur by the overlapping sequences that act as relevant primers during the second round of PCR. **(C)** PCR with a nested set of primers to further amplify the desired DNA sequence.

Here, in the first round of PCR, 5' and 3'-untranslated regions (UTR) of *FAE1* gene were individually amplified from *M. oryzae* WT genomic DNA, while hygromycin phosphotransferase (*HPT*; selectable marker) gene cassette, consisting of TrpC promoter and terminator sequences, was amplified from a pBS(KS)-HPT vector (already available in the lab). These PCR products were confirmed for the desired size (Fig. 3.2.2A) and then subsequently joined by a second round of PCR, giving rise to an expected ~5.1 kb DNA fragment, along with other non-specific amplification products (Fig. 3.2.2B). This sample was further subjected to a third round of PCR using nested primers to obtain a specific amplification product of ~3.8 kb (Fig. 3.2.2C). This recombinant PCR product was further purified by Na-acetate/ethanol precipitation and confirmed by RE digestion (Fig. 3.2.2D).

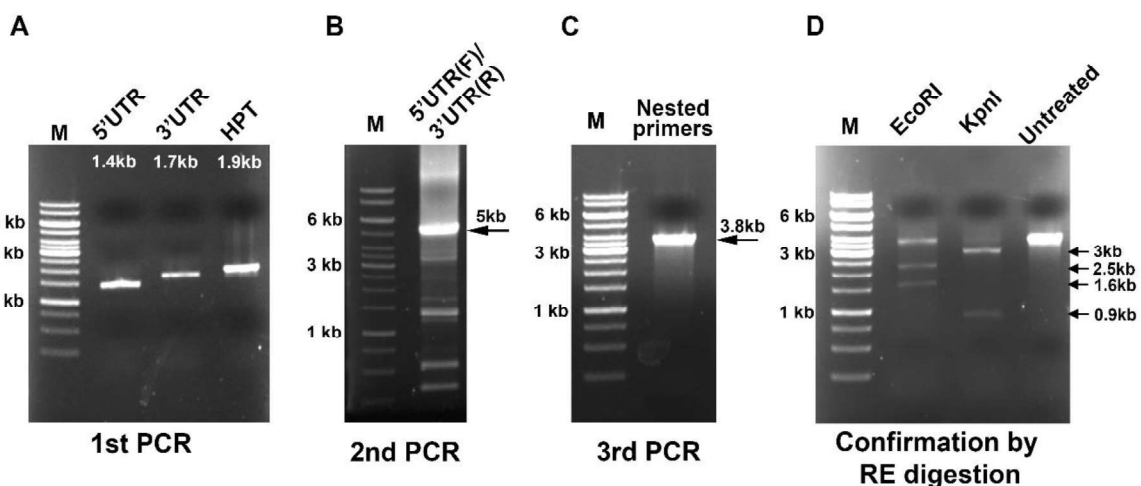


Figure 3.2.2. Generation of *FAE1*-deletion cassette by double-joint PCR approach and its confirmation. (A – C) Agarose gel electrophoresis showing amplification products obtained during three sequential rounds of PCR. Numbers on the left-hand side of each gel denote representative sizes of the DNA fragments in the marker (M); whereas that on the right-hand side (B & C) or marked on each lane (A) denotes the desired size of the DNA fragment obtained during each round of PCR. **(D)** Confirmation of PCR product obtained in

C) by two different RE digestion reactions. Numbers on the left-hand side denote representative sizes of the DNA fragments in the marker (M), whereas those on the right-hand side show desired sizes of the DNA fragments obtained upon *EcoRI* (2.5 and 1.6 kb) or *KpnI* (3.0 and 0.9 kb) digestion.

Primers and PCR conditions used for generation of *FAE1*-deletion construct are listed below in Table 3.2.1 and 3.2.2 respectively.

Primer	Sequence (5' → 3')
FAE-8737-5'UTR(F)	TCAGTATGGCCCACCTACCCAA
FAE-8737-5'UTR(R)	ctcctcaatatcagttaacgtcTTGAGGCAGCTCTCTGGGAACG
FAE-8737-3'UTR(F)	gaaaattccgtcaccagccctggCAACAGGGGGCGGGGACTCATA
FAE-8737-3'UTR(R)	AAAGTAGGGGGAAGCCGTCAGC
FAE-8737-NST(F)	TGGAATCAGTGCCGTCAGAA
FAE-8737-NST(R)	AGGGGAGCCTGAAGATATGGA
pTrpC-HPT-tTrpC(F)	GACGTAACTGATATTGAAG
pTrpC-HPT-tTrpC(R)	CCAGGGCTGGTGACGGA

Table 3.2.1: List of oligonucleotide primers used for generation of *FAE1*-deletion construct. Sequences in lower case denote overlapping-sequences used for joining 5'UTR, HPT-cassette and 3'UTR fragments by double-joint PCR.

Product	Size	Template	Primers (F/R)	Key parameters
First Round PCR (amplification of individual DNA fragments)				
5'UTR	1461 bp	WT gDNA	FAE-8737-5'UTR	Annealing – 60 °C, 0.5' Extension – 72 °C, 2' No. of cycles – 30 Reaction vol. – 20 µL
3'UTR			FAE-8737-3'UTR	
HPT cassette	1885 bp	pBS(KS)-HPT	pTrpC-HPT-tTrpC	
Second Round PCR (joining of DNA fragments from first round PCR)				
5'UTR-HPT-3'UTR	5054 bp	1:10 diluted: 5'UTR (2 µL) +3'UTR (3 µL) +HPT (3 µL)	FAE-8737-5'UTR(F) & FAE-8737-3'UTR(R)	Annealing – 56 °C, 2' Extension – 72 °C, 3' No. of cycles – 35 Reaction vol. – 25 µL
Third Round PCR (PCR with nested primers for specific amplification)				
<i>FAE1</i> -deletion cassette	5'UTR(957bp), HPT(1885bp), 3'UTR(963bp) = 3805 bp	2 µL of 1:10 ⁴ diluted second round PCR product	FAE-8737-NST	Annealing – 60 °C, 0.5' Extension – 72 °C, 3' No. of cycles – 30 Reaction vol. – 25 µL

Table 3.2.2: PCR conditions used for generation of *FAE1*-deletion cassette. During all the rounds of PCR, 1- 2 units of XT5 DNA polymerase, 1× XT-5A buffer, 0.2 mM dNTPs and 1 µM primers, each per tube were used.

FAE1 gene-deletion cassette was then introduced into WT *M. oryzae* by a standard protoplast transformation method (described in Chapter 2) to achieve a targeted replacement of *FAE1* gene with *HPT* gene cassette via homologous recombination (Fig. 3.2.3A). Fungal transformants were first selected on YEG agar plates containing 300 µg/mL hygromycin, followed by a secondary selection on media containing 200 µg/mL hygromycin. Higher concentration of hygromycin during primary selection was used to reduce the chances of getting any false positive transformants. Collectively, 72 transformants growing on secondary selection media were obtained from three independent rounds of protoplast transformation.

3.2.1.2 Molecular analysis and confirmation of *FAE1*-deletion mutant (*fae1Δ*)

The hygromycin-resistant transformants were further screened by a locus-specific PCR, where one out of a total 72 transformants showed the desired size of PCR product (Fig. 3.2.3B). The selected transformant was further analysed by RT-PCR to confirm the absence of any *FAE1* transcript. Here, the first-strand cDNA was synthesized using total RNA isolated from the selected transformant along with that from WT and an ectopic transformant, followed by a PCR with *FAE1* ORF-specific primers (FAE-8737-ORF(F): 5'ATGAGATCCTCACTCTTTGCGG3' and FAE-8737-ORF(R): 5'CTACACGCACTGCCAGCTAT3'). As expected, no *FAE1* transcript was detected in the selected transformant when compared with the WT or an ectopic transformant (Fig. 3.2.3C).

Next, the selected transformant was checked by Southern blot hybridization for the copy number and site-specific integration of the *HPT* gene cassette at the *FAEI* locus. Here, genomic DNA isolated from the WT, *fae1*Δ and ectopic transformant was subjected to *Pst*I digestion. Alongside, a DNA stretch for probe was prepared by PCR-amplification of *HPT* ORF fragment (897 bp region) from the *FAEI*-deletion cassette (obtained in section 3.2.1), using HygN primers (Forward – 5' AGGGCGAAGAATCTCGTGCTT 3' and Reverse – 5' CCACTATCGGCGAGTACTTCT 3'), 30 thermal-cycling reactions with 60 °C annealing temperature and 72 °C for 1 min extension at each cycle. This amplified product was then purified by gel-extraction and subsequently used for labelling and DNA detection using Alkphos Direct labelling and detection kit (GE Healthcare Ltd., UK as described in Chapter 2). Southern blot hybridization analysis showed two bands of expected sizes (~3.8 and ~4.5 kb) in the selected transformant, thereby confirming the replacement of *FAEI* ORF with a single copy of *HPT* gene cassette (Fig. 3.2.3D). This *FAEI* gene deletion transformant was used for subsequent phenotypic characterization and is hereafter referred as '*fae1*Δ' mutant.

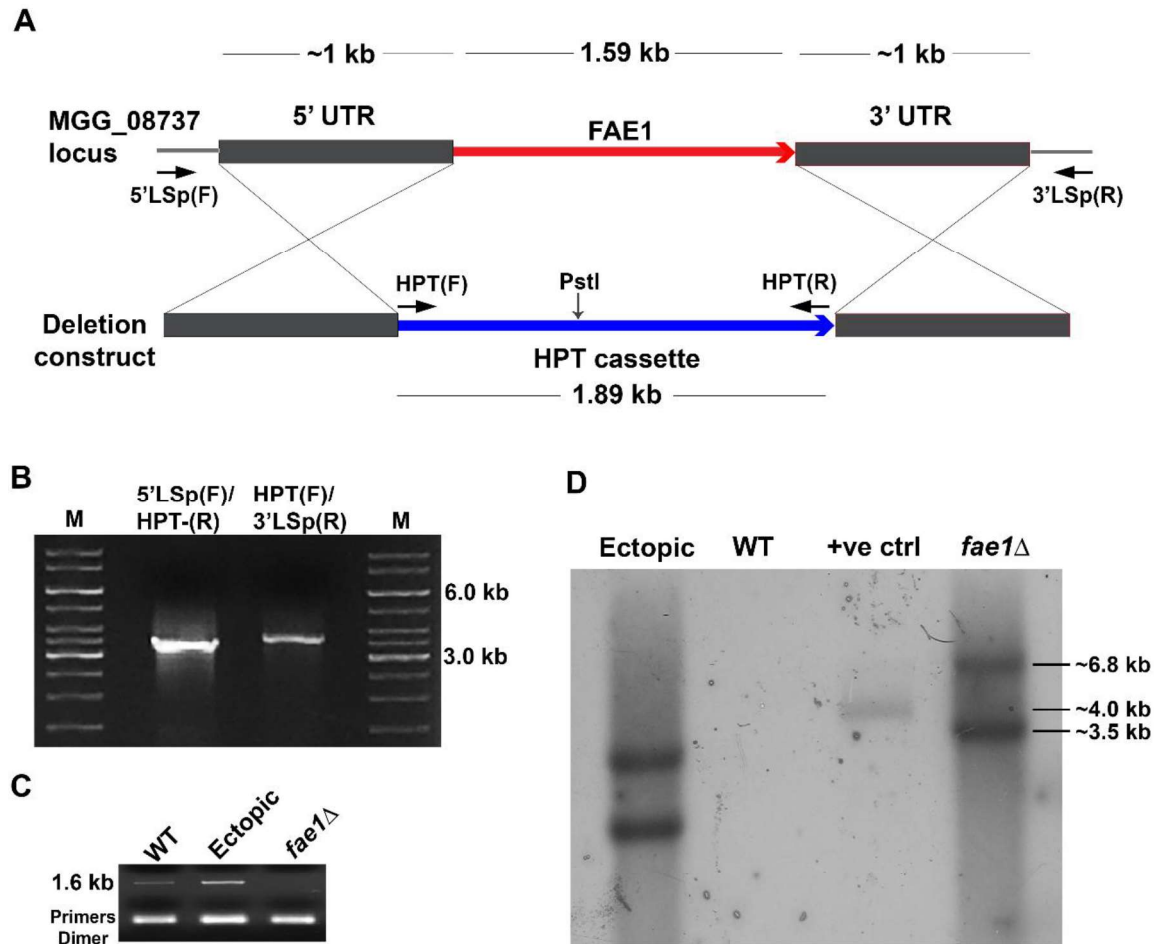


Figure 3.2.3. Molecular characterization of the *FAE1*-deletion (*fae1Δ*) strain. (A) Schematic representation of replacement of the 1.59 kb *FAE1* ORF (MGG_08737) with a 1.89 kb Hygromycin Phosphotransferase (HPT) gene cassette via homologous recombination. **(B)** Confirmation of a hygromycin-resistant fungal transformant (*fae1Δ*) using locus-specific PCR (5' LSp(F) and 3' LSp(R) primer positions, outside of the gene-deletion construct, are denoted with arrows in A). The numbers on the right-hand side denote the sizes of the representative fragments in the DNA marker (M). The expected amplification products with primer pairs 5'-LSp(F)/ HPT(R) and HPT(F)/3'-LSp(R) corresponding to ~3.4 kb and ~3.8 kb, respectively, were obtained from the transformant. **(C)** Expression of *FAE1* in the WT or *fae1Δ* strain confirmed by RT-PCR. The expected cDNA product size is marked on the left. **(D)** Southern blot analysis of the WT and *fae1Δ* strains. Genomic DNA was digested with *PstI* (position marked in A) and hybridized with labelled *HPT* gene cassette as a probe. An undigested deletion cassette (~4.0 kb, as shown in A) was used as a positive control for confirming the efficiency of hybridisation by a labelled probe. Numbers on the right-hand side denote the fragment sizes.

3.2.2 *fae1*Δ mutant shows normal vegetative growth and asexual conidial development

3.2.2.1 Vegetative growth

To assess the growth characteristics of the *fae1*Δ, a 10-day old mycelial culture grown on prune agar (PA) plates was compared to that of the WT. Visual observation showed that colony morphology and pigmentation was similar in both the strains (Fig. 3.2.4A). Moreover, the radial mycelial growth, in terms of colony diameter (at 10 dpi), of the *fae1*Δ (7.17 ± 0.06 cm) was found to be comparable to that of the WT (7.37 ± 0.06 cm; P -value = 0.205; Fig. 3.2.4B).

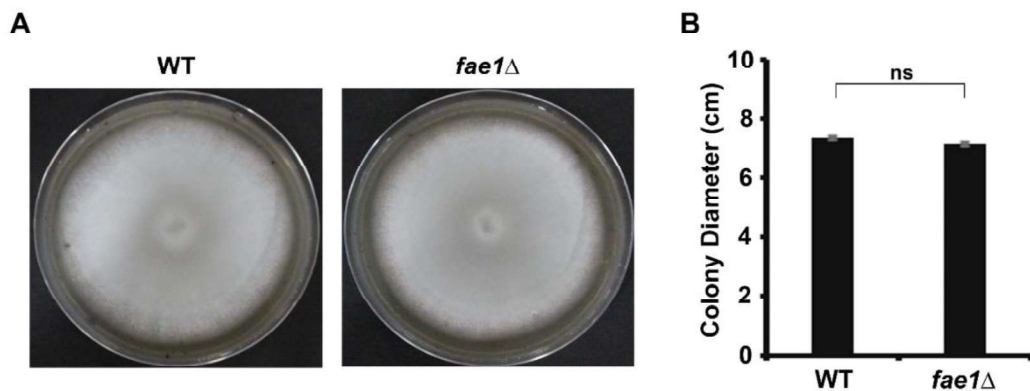


Figure 3.2.4. Vegetative growth of the *fae1*Δ mutant. Vegetative growth of the WT or *fae1*Δ on prune agar plates at 10 dpi (A) and measurement of diameters of colonies of both the strains (B). Data represents mean \pm s.d.m. from the experiments repeated thrice.

3.2.2.2 Asexual development (conidiation)

Total conidiation was determined by harvesting asexual conidia from vegetative culture on PA plates at 10 dpi. Conidia harvested from the WT and *fae1*Δ were counted using a Neubauer chamber under a bright field microscope. Number of conidia obtained from the *fae1*Δ ($102.2 \pm 12.2 \times 10^2$ conidia/cm²) was found comparable to that of the WT (99.1 ± 7.4

$\times 10^2$ conidia/cm²) (P -value = 0.737; Fig. 3.2.5). Moreover, conidial morphology of the *fae1* Δ , showing normal three-celled conidia, was similar to that of the WT.

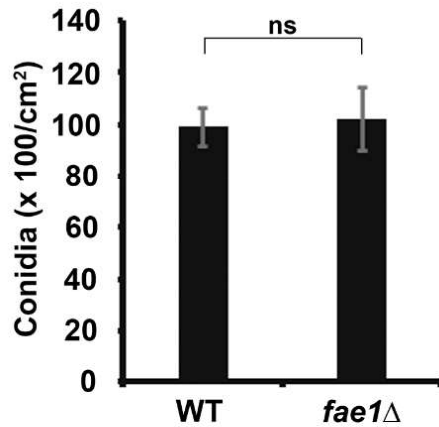


Figure 3.2.5. Asexual development (conidiation) of *fae1* Δ mutant. A bar graph depicting total conidiation assessed by counting the number of conidia harvested at 10 dpi from the WT or *fae1* Δ culture grown on PA plates. Data represents mean \pm s.d.m. from three independent experiments. ns, not significant.

3.2.3 Fae1 function is not required for the appressorial development in *M. oryzae*

Appressorium being a specialised and an essential infection structure in *M. oryzae*, and given a significant increase in the *FAE1* transcript levels at the pre-invasive stage (12 hpi; as determined in section 3.1.7.2), appressorial development was studied to check whether deletion of *FAE1* had any effect therein. Appressorial assay was carried out on an artificial hydrophobic surface (hydrophobic glass coverslips) using both WT and *fae1* Δ under identical conditions and results were analysed at 24 hpi. Microscopic observation showed that the loss of Fae1 function did not affect the formation of the infection structure, where the morphology of the *fae1* Δ appressoria was comparable to that of the WT (Fig. 3.2.6A). Furthermore, the % appressoria formed by the *fae1* Δ (81.7 ± 0.82 %) was found similar to WT (83.0 ± 1.5 %; P -value = 0.289; Fig. 3.2.6B).

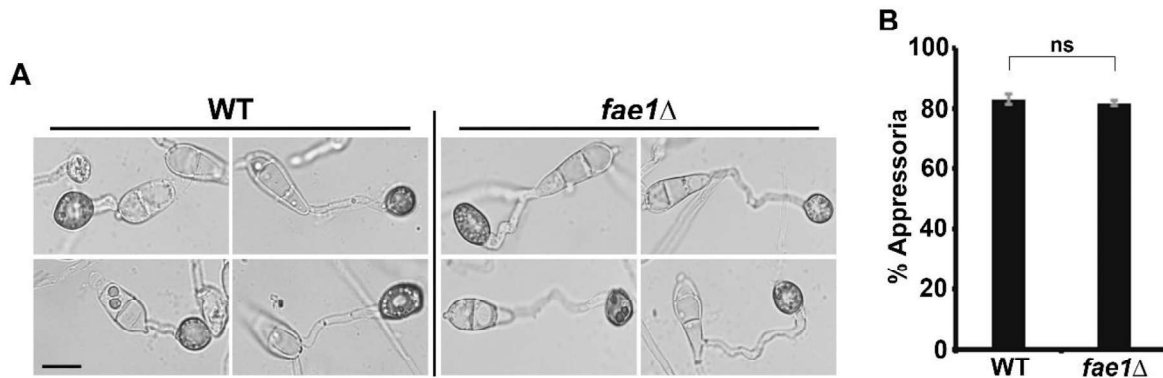


Figure 3.2.6. Pathogenic (appressorial) development in the absence of Fae1 function in *M. oryzae*. (A) Micrographs showing appressorial development, on an inductive glass surface, in the WT or *fae1Δ* strain, at 24 hpi. Scale bar, 10 μ m. (B) A quantitative analysis of appressorial development in the WT or *fae1Δ* at 24 hpi. Data represents mean \pm s.d.m. from three independent experiments, with at least 100 appressoria each observed for quantification. ns, not significant.

Altogether, these results suggest that Fae1 does not play an important role during host-independent stages of fungal development such as vegetative growth, asexual development and appressorium formation in *M. oryzae*.

3.2.4 Development of blast disease by *M. oryzae* is impaired in the absence of Fae1 function

Infection ability of the *fae1Δ*, compared to WT, was checked by inoculating conidia onto 3–4-week-old rice plants and incubated under humid conditions for 5–6 days. Development of any disease symptoms was monitored regularly. Interestingly, plants inoculated with *fae1Δ* did not show typical necrotic blast disease lesions, while plants inoculated with WT developed characteristic disease lesions (Fig. 3.2.7A). Further, a similar defect in causing infection by the *fae1Δ* was also observed on another host plant barley (Fig. 3.2.7B).

This indicated that Fae1 plays an important role in pathogenesis of *M. oryzae*. It was therefore important to check any effect of *FAE1*-deletion on other pathogenic stages such as host invasion and colonisation, prior to necrotrophic phase of plant infection.

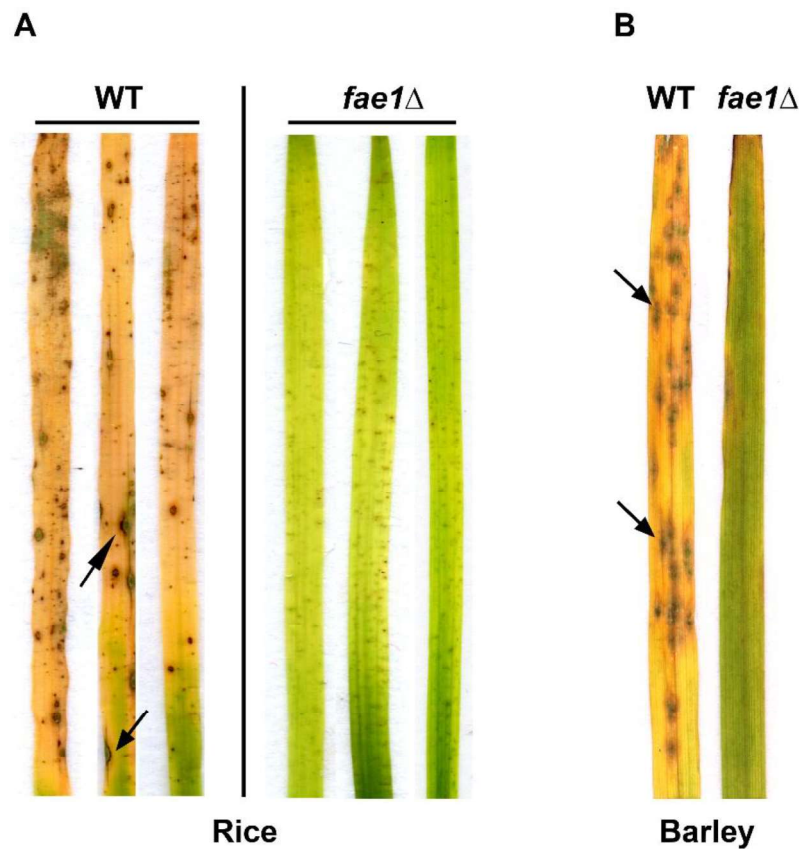


Figure 3.2.7. Plant infection assay depicting blast disease outcome from rice (A) or barley (B) plants inoculated with WT or *fae1Δ* conidia. The representative leaves were detached and photographed after 6 dpi. Arrows mark the typical blast disease lesions.

3.2.5 Fae1 is required specifically for host colonisation by *M. oryzae*

3.2.5.1 Invasive growth is impaired in the *fae1*Δ mutant

Penetration followed by tissue colonization is a crucial step for successful infection by *M. oryzae*. In order to further investigate the impaired pathogenesis in the *fae1*Δ strain, the invasive growth was studied compared to WT. Here, rice leaf sheath tissue, which facilitates microscopic observation due to its optical clarity, was used to study host penetration and colonisation. Rice sheaths were inoculated with conidia harvested from WT or *fae1*Δ and incubated under humid conditions. Sheaths were then observed for any invasive growth at ~48 hpi under a bright field microscope. Interestingly, most of the *fae1*Δ appressoria, unlike that of WT, were unable to form visible primary invasive hyphae in the rice sheath tissue (Fig. 3.2.8A). Moreover, importantly, a few *fae1*Δ appressoria that could form primary invasive hyphae were found to be restricted to the first invaded host cell and failed to elaborate further to the adjacent neighbouring cells (Fig. 3.2.8A). To test whether *fae1*Δ exhibits any delayed host colonization, the invasive growth was further checked at 96 hpi. However, even after prolonged incubation, *fae1*Δ mutant failed to colonize the plant tissue as compared to profuse invasive hyphal growth of the WT by then (Fig. 3.2.8C). These observations are in line with the hypothesis that Fae, and CWDEs in general, likely play an important role in cell-to-cell spread of the fungus within the host tissue, and subsequent necrotrophic growth (Zheng et al., 2009). Invasive growth of the *fae1*Δ was also checked on other hosts such as barley and wheat; however, a similar host-invasion defect was observed, as found on rice (Fig. 3.2.8D).

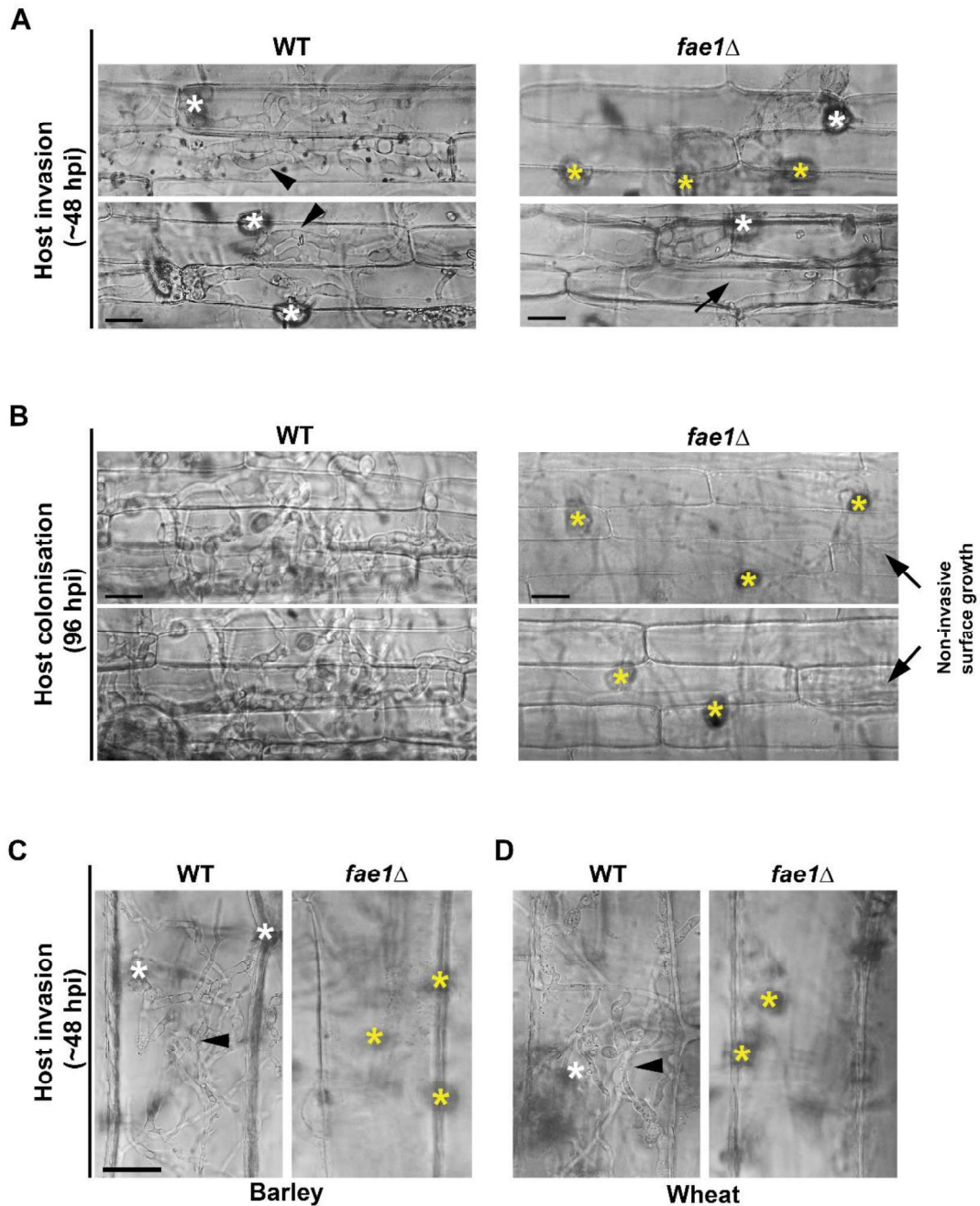


Figure 3.2.8. The *fae1Δ* strain shows defects in host invasion and colonisation. Micrographs showing host invasion at ~48 hpi (**A**) and subsequent colonisation at 96 hpi (**B**) of the WT or *fae1Δ* mutant. Barley (**C**) or wheat (**D**) leaf sheath inoculated with the WT or *fae1Δ* conidia and observed under the bright-field optics at ~48 hpi. For all the micrographs, asterisks denote appressoria, while arrowheads mark the invasive hyphae spreading to the neighbouring host cells. Yellow asterisks mark the non-invading appressoria and arrow depicts the invasive hyphae restricted to the first invaded host cell. Scale bar, 10 μ m.

Since a significant percentage of mutant appressoria did not show visible invasive hyphae, it was important to check whether the *fae1* Δ strain had lost the ability to breach the host leaf cuticle via penetration peg. This was studied by determining the sites of appressorium penetration, which are marked by deposition of callose, a plant polysaccharide that gets accumulated locally at the site of wound or damage. Here, the rice sheaths were inoculated with conidia from *fae1* Δ or WT strain followed by 36 h incubation under humid conditions. These sheaths were then de-colored by an overnight methanol treatment, followed by aniline blue staining for 30-60 min at room temperature. After staining, sheaths were observed under an epifluorescence microscope to check for fluorescence from any callose deposited at the site of appressorium penetration. Interestingly, a considerable proportion of *fae1* Δ appressoria, compared to WT, was efficiently able to breach the leaf cuticle, as visualized by callose deposition (Fig. 3.2.9).

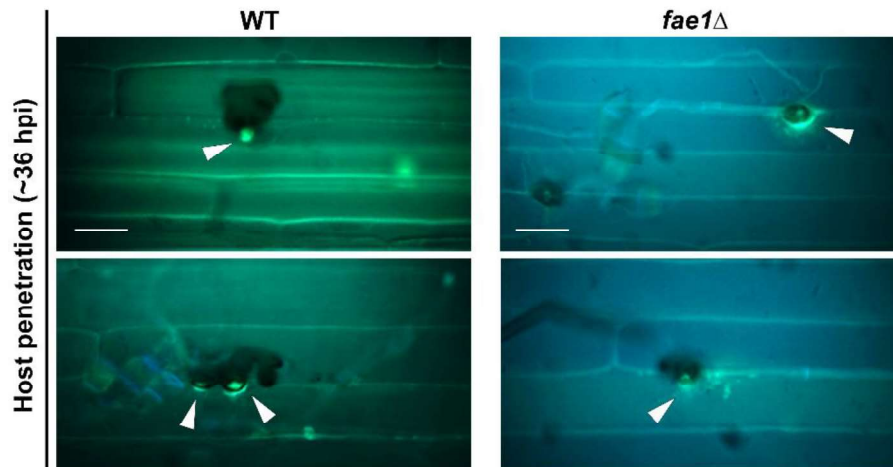


Figure 3.2.9. Host penetration assay by aniline blue staining. Micrographs showing rice leaf sheath penetration, marked by aniline blue stained callose deposits (arrowheads), by the WT or *fae1* Δ at 36 hpi. Scale bar, 10 μ m.

Altogether, these findings show that the Fae1 function is not required for penetrating the host cuticle but for colonisation of the host tissue. The significant defect in pathogenesis of the *fae1*Δ mutant could be attributed to impaired host invasion and colonisation.

3.2.5.2 Genetic complementation of the *fae1*Δ mutant rescues its host invasion defect

To validate the effect of *FAE1*-deletion on impaired pathogenicity of *M. oryzae*, a genetic complementation strain of *fae1*Δ mutant was constructed by introducing a native copy of *FAE1* ORF along with its 5'UTR, followed by its phenotypic characterization. Here, a full-length genomic sequence of *M. oryzae* *FAE1* ORF (MGG_08737) along with 5'-UTR (~1.5 kb) was amplified by PCR using FAE-8737-5'UTR(F) and FAE-8737-NST(R) primers (Table 3.2.1). The amplified PCR product was first cloned at *EcoRV* site (blunt-end cloning) in a basic pBluescript(KS⁺) vector (Fig. 3.2.10A), which facilitates blue-white colonies based screening. Plasmid was then isolated from the white colonies and screened by *HindIII* digestion for desired (sense) orientation of the cloned 5'UTR-*FAE1* ORF sequence (Fig. 3.2.10B). The recombinant plasmid, thus obtained, was digested with *EcoRI* and *XbaI* and the released DNA fragment was subsequently cloned at *EcoRI/XbaI* sites in pFGL889-*ILV2*^{SUR}-based pFGL1010 vector (Yang and Naqvi, 2014; Addgene plasmid # 119081; Fig. 3.2.10C). The cloned 5'UTR-*FAE1* ORF sequence was confirmed by *HindIII*-digestion of the recombinant plasmid and was designated as pRPL049 (Fig. 3.2.10D). Furthermore, the sequence for complementation was PCR-amplified from the pRPL049 using LB-F1 (5'-TGCGGACGTTTTTAATGTACTG-3') and RB-R1 (5'-GAAACGACAATCTGATCCAAGC-3') primers. The amplified PCR product was again confirmed by RE-digestion and purified by gel extraction (Fig. 3.2.10E), followed by its

introduction into *fae1*Δ strain by protoplast transformation method (Chapter 2). As described previously (Yang and Naqvi, 2014), the transformants were selected on Basal Medium (BM) containing 100 μg/mL chlorimuron ethyl, as only those with *ILV2*^{SUR}-5'UTR-*FAE1* integrated at the native *ILV2* locus will be able to grow on this selection medium. A chlorimuron ethyl resistant transformant, thus obtained, was confirmed by locus-specific PCR using *ILV2*-5'UTR (5'- TTGTCATCGTCTGACAGGTC) and *FAE*-8737-5'UTR-R (Table 3.2.1) primers. This transformant was further analysed by RT-PCR, wherein *FAE1* transcript was obtained (Fig 3.2.10E and 3.2.10F). This genetic complementation transformant, after molecular confirmation, designated as *fae1*Δ/*FAE1* was used for subsequent phenotypic characterization.

Genetic complementation strain (*fae1*Δ/*FAE1*) was first evaluated for its infection ability on rice or barley plants. Conidia isolated from WT, *fae1*Δ or *fae1*Δ/*FAE1* strains were inoculated each on rice/barley whole-plants or detached barley leaves, and development of any disease symptoms was monitored regularly. Importantly, plants inoculated with the genetic complementation strain (*fae1*Δ/*FAE1*) developed typical disease lesions like that of WT (Fig. 3.2.11). The *fae1*Δ mutant, consistent with earlier observation, failed to develop typical blast disease lesions (Fig. 3.2.11). Thus, introduction of native *FAE1* gene copy could rescue the pathogenicity defect, and thereby genetically complement the *fae1*Δ mutant.

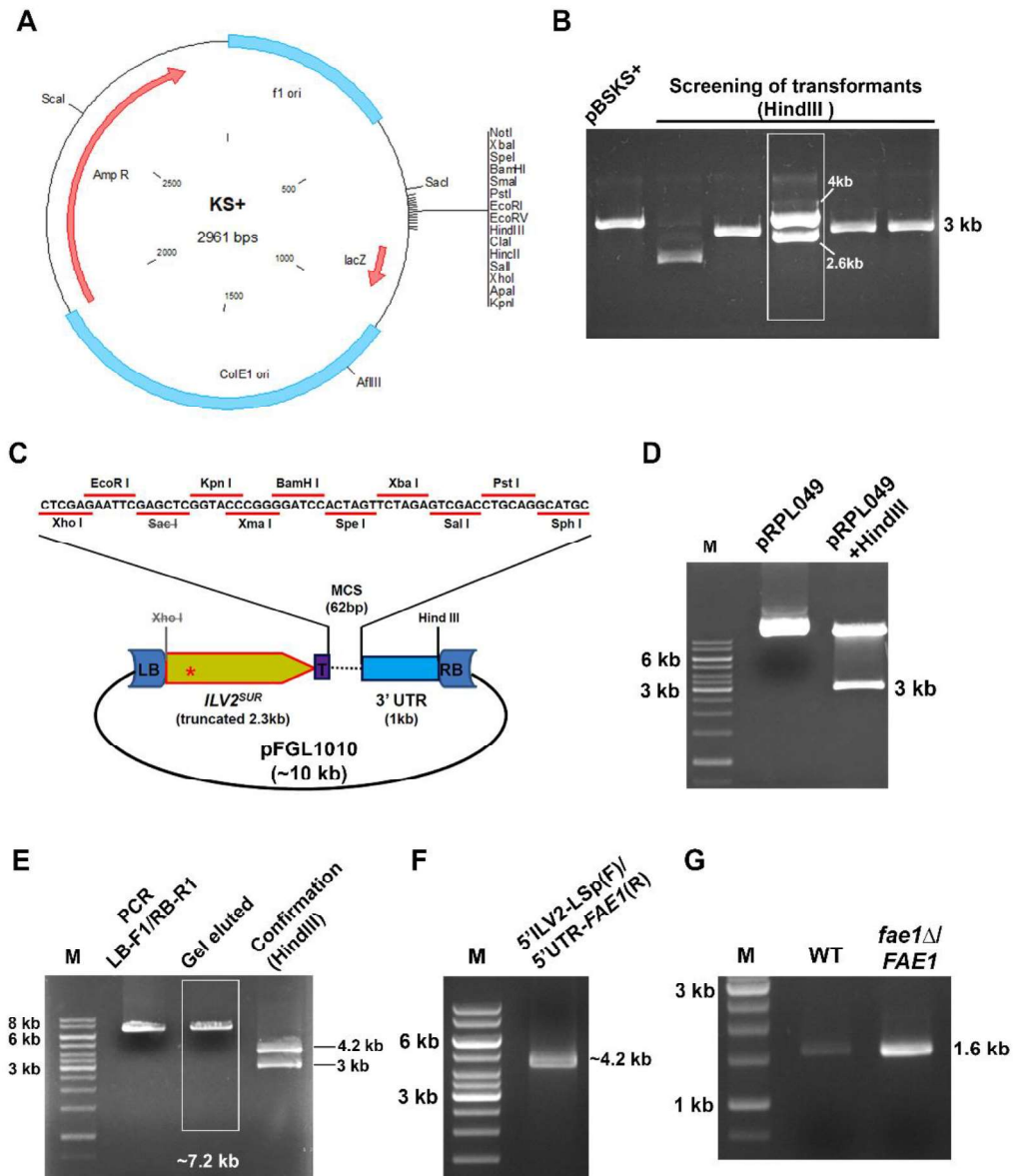


Figure 3.2.10. Generation of construct for genetic complementation and molecular analysis of *fae1*Δ/*FAE1* strain. (A) Map of pBluescript KS+ vector. (B) Screening of ampicillin-resistant *E. coli* transformants (white colonies) by *Hind*III digestion. Lane marked with a box shows expected DNA fragments (4.0 and 2.6 kb) obtained upon RE-digestion corresponding to desired recombinant plasmid. (C) Map of pFGL1010 vector. (D) Confirmation of recombinant plasmid pRPL049 containing 5'UTR-*FAE1*ORF by *Hind*III digestion, generating a desired 3 kb DNA fragment. (E) Preparation of final sequence, for complementation, by PCR amplification (with LB-F1/RB-R1 primers), followed by its purification (gel elution). Lane marked with white box shows a desired 7.2 kb DNA fragment obtained after gel elution, confirmed by *Hind*III digestion and subsequently used for fungal transformation. M (D – G) denotes standard 1 kb DNA ladder and numbers on the left-hand

side show sizes of the corresponding DNA bands. **(F)** Confirmation of genetic complementation (*fae1Δ/FAE1*) by performing *ILV2* locus-specific PCR. Forward primer, 5'ILV2-LSp(F) binds upstream to the *ILV2* locus in the genomic region (outside of complementation construct), whereas, the reverse primer, 5'UTR-FAE1(R) binds to the region within the complementation construct. Expected ~4.2 kb PCR product was obtained, confirming the site-specific integration of the complementation construct. **(G)** Expression of *FAE1* in the WT or *fae1Δ/FAE1* strain confirmed by RT-PCR. The expected fragment size is denoted on the right-hand side. The sizes of the characteristic fragments in the DNA marker (M) are mentioned on the left-hand side.

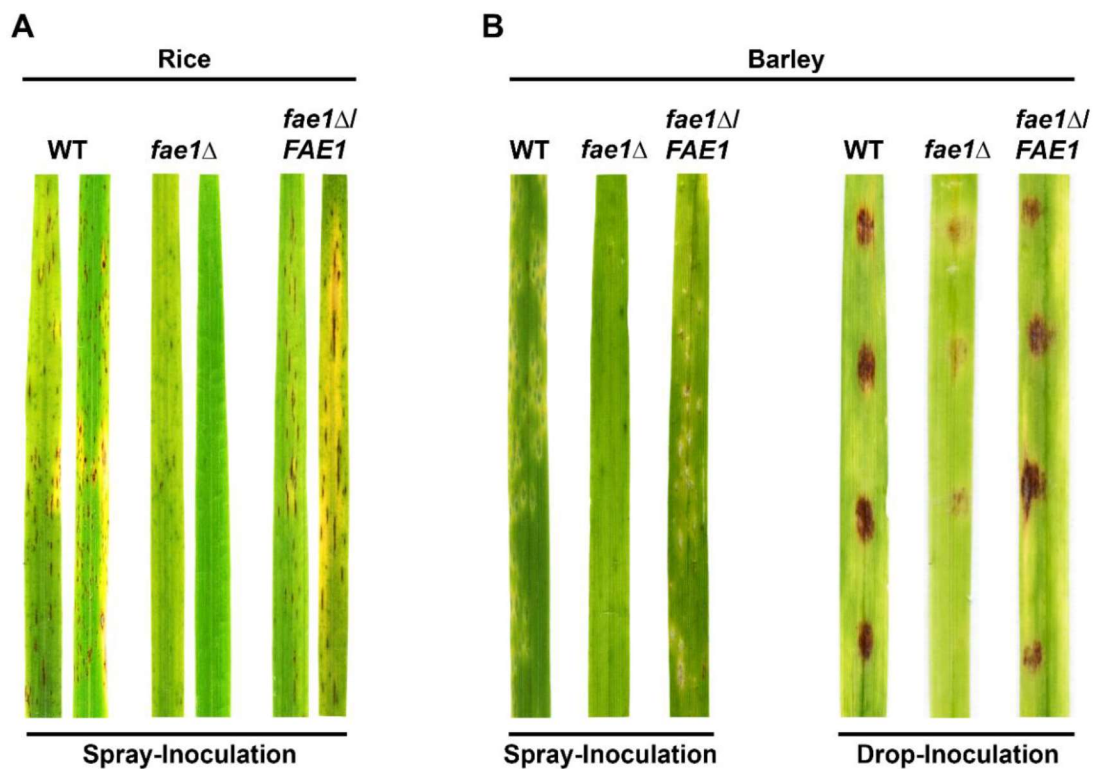


Figure 3.2.11. Infectivity of the WT, *fae1Δ* or *fae1Δ/FAE1* on rice whole-plants **(A)** or barley whole plants or detached leaves **(B)**. The leaves were imaged on 5-6 dpi.

Next, having found that the complementation strain (*fae1Δ/FAE1*) could rescue the pathogenicity defect of *fae1Δ* mutant, its host invasion ability was tested. To evaluate this, rice sheaths were inoculated with conidia harvested from WT, *fae1Δ* or *fae1Δ/FAE1* strains and incubated under humid conditions. Invasive hyphal growth was then checked and

quantified at ~48 hpi, as performed earlier (section 3.2.5.1). Quantitative analysis with three independent set of samples, revealed that while 77.33% (\pm 5.41%) of WT appressoria formed visible invasive hyphae, only 3.28% (\pm 0.25%) of *fae1* Δ appressoria were able to invade and form primary invasive hyphae, which failed to further colonise the plant tissue (Fig. 3.2.12A and 3.2.12B). Importantly, 56.88% (\pm 2.29%) of *fae1* Δ /*FAE1* appressoria formed invasive hyphae, which was significantly higher compared to *fae1* Δ mutant, and thereby rescued its host invasion defect (P -value = 0.0003; Fig. 3.2.12A and 3.2.12B).

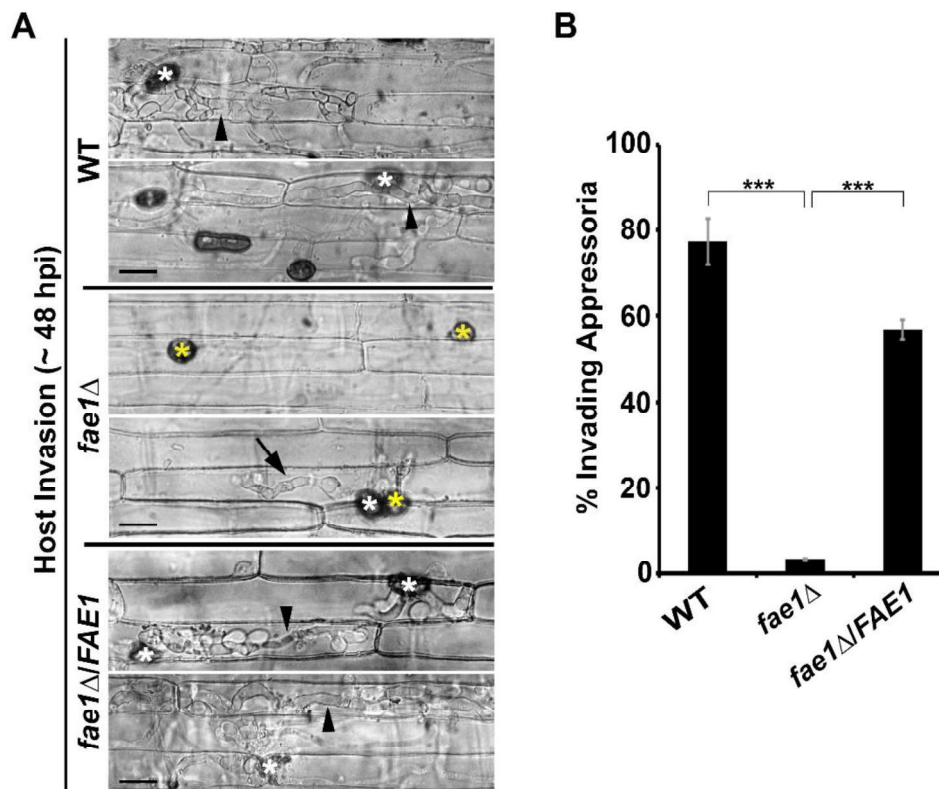


Figure 3.2.12. Micrographs showing host invasion (~48 hpi) ability of the WT, *fae1* Δ or *fae1* Δ /*FAE1* strains (A). Asterisks mark appressoria, while arrowheads depict the invasive hyphae. Yellow asterisks mark the non-invading *fae1* Δ appressoria and the arrow depicts the invasive hypha restricted to the first invaded host (rice sheath) cell. Scale bar, 10 μ m. (B) A bar chart depicting percentage of appressoria invading the rice sheath inoculated with the WT, *fae1* Δ , or *fae1* Δ /*FAE1* strain. Data represents mean \pm s.d.m. from three independent experiments, with at least 100 appressoria each observed for quantification. ***, $P < 0.001$; ns, not significant.

Altogether, the results show that the Fae1 function alone is specifically required for host penetration and colonisation towards successful blast disease.

3.2.5.3 Exogenous addition of the products of Fae enzyme action rescues the host invasion defect of the *fae1*Δ mutant

It has been reported that the blast fungus utilizes stored lipids for deriving energy via β -oxidation in the mitochondria and peroxisomes (Wang et al., 2007; Patkar et al., 2012), which might support initial appressorial development and host penetration. Further, it is possible that the plant cell wall carbohydrates released after CWDEs activity could act as an energy source for the fungus at the host-pathogen interface and facilitate its entry and/or elaboration into the host. Fae enzyme action on plant cell wall would release ferulic acid and polysaccharide molecules. Feruloyl esterases in *Aspergillus niger* act synergistically, with other CWDEs like cellulases, xylanases and pectinases, to degrade the complex plant cell wall carbohydrates (Faulds and Williamson, 1995). In *M. oryzae*, endo-xylanases (Nguyen et al., 2011) and cellulases (Vu et al., 2012) are shown to be important in host-penetration and virulence of the blast fungus. Considering all this, it was interesting to study whether the sugar or ferulic acid released from Fae and other CWDE-mediated plant cell wall digestion could support the invasive hyphal growth of *fae1*Δ mutant.

To investigate whether exogenous addition of these compounds (i.e., sugar or ferulic acid) would support the *fae1*Δ mutant in efficient host tissue colonisation; an *in vitro* host-invasion assay of the WT and *fae1*Δ mutant in the presence of these compounds, individually or in combination, was performed. Here, different concentrations of glucose (2%, 1.5%, 1% and 0.5%) or ferulic acid (100 mM, 50 mM and 10 mM) or their combinations (i.e., 1% glu + 10 mM FA and 0.5% glu + 10 mM FA) was exogenously added

at ~22 hpi, i.e., before the onset of host penetration and to avoid any interference in appressorial development which is associated with a nutrient-deficient condition. Imaging and quantification of the invasive hyphal growth, if any, was carried out at ~48 hpi. Interestingly, treatment with ferulic acid or glucose individually enabled an efficient invasive growth of the *fae1* Δ mutant, in a dose-dependent manner (Fig. 3.2.13A and 3.2.13B). While 2% glucose could significantly restore the host invasion ($74.8 \pm 9.8\%$) by the *fae1* Δ , comparable to that of the WT ($75.4 \pm 8.3\%$), other decreasing concentrations of glucose such as 1.5%, 1% and 0.5% could also support the invasive growth of the *fae1* Δ to $50.2 \pm 9.7\%$ (P -value = 0.007), $30.5 \pm 5.5\%$ (P -value = 0.02) and $17.1 \pm 3.2\%$ (P -value = 0.036) respectively (Fig. 3.2.13A and 3.2.13B). Likewise, host invasion ability of the *fae1* Δ was improved upon exogenous addition of 100 mM ($53.2 \pm 5.9\%$) and 50 mM ($29.3 \pm 5.3\%$) ferulic acid (P -value = 0.003; Fig. 3.2.13A and 3.2.13B). However, exogenous addition of 10 mM ferulic acid could show only a marginal increase in host invasion ($7.1 \pm 2.8\%$) by the *fae1* Δ mutant. Here, host invasion of WT, as a control, was also checked in the presence of glucose or ferulic acid, whereby, its host invasion ability was found to be unaltered (Fig. 3.2.14A). A dose-dependent beneficial effect of glucose or ferulic acid could also be observed on the infection ability of the *fae1* Δ on detached rice leaves (Fig. 3.2.14B). This observation was further substantiated by the whole-plant infection assay wherein the rice plants inoculated with the *fae1* Δ mutant showed development of disease lesions upon exogenous addition of 2% glucose or 100mM ferulic acid (Fig. 3.2.14C). Furthermore, to check any synergistic effect of these two molecules, a host invasion assay was performed where the *fae1* Δ mutant was treated with two different combinations of glucose and ferulic acid (viz. 1% glu + 10 mM FA and 0.5% glu + 10 mM FA). However, neither of these combinations showed any remarkable improvement in host invasion by the *fae1* Δ , when

compared to the WT or the mutant treated with 2% glucose alone (Fig. 3.2.13A and 3.2.13B).

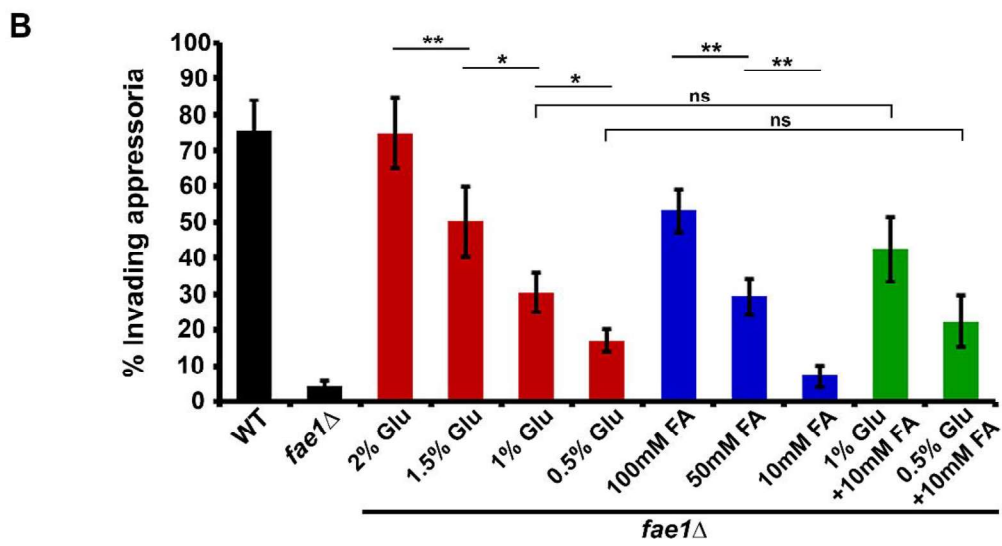
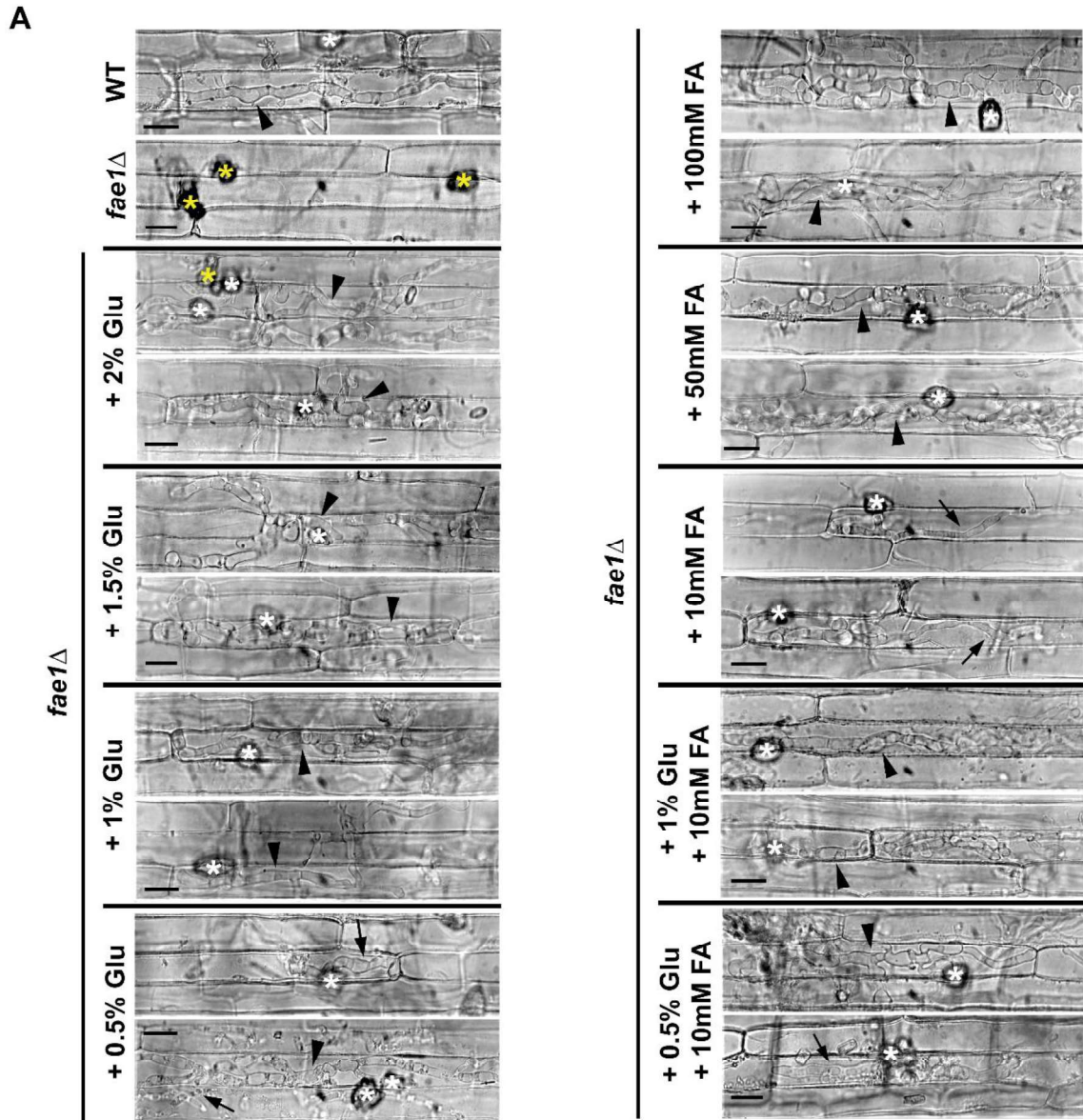


Figure 3.2.13. Exogenously added glucose or ferulic acid support host invasion in the *fae1Δ* in a dose-dependent manner. (A) Rice leaf sheath inoculation assay showing host invasion ability of the WT, *fae1Δ* or *fae1Δ* supplemented with varying concentrations of glucose (2%, 1.5%, 1% and 0.5%), ferulic acid (100 mM, 50 mM and 10 mM) or their combinations (1% glu + 10 mM FA and 0.5% glu + 10 mM FA), which were added at 22 hpi. The results were observed at 48 hpi. White and yellow asterisks mark the invading and non-invading appressoria, respectively. Arrows depict invasive hypha restricted to the first host cell invaded, while arrowheads represent invasive hyphae spreading to the neighbouring cells. Scale bar, 10 μm. **(B)** A bar chart depicting percentage appressoria invading rice sheath inoculated with either the WT, *fae1Δ* or *fae1Δ* supplemented with different concentrations of glucose, ferulic acid or their combinations. Data represents mean ± s.d.m. from three independent experiments, with at least 100 appressoria each observed for quantification. *, $P < 0.05$; **, $P < 0.01$; ns, not significant.

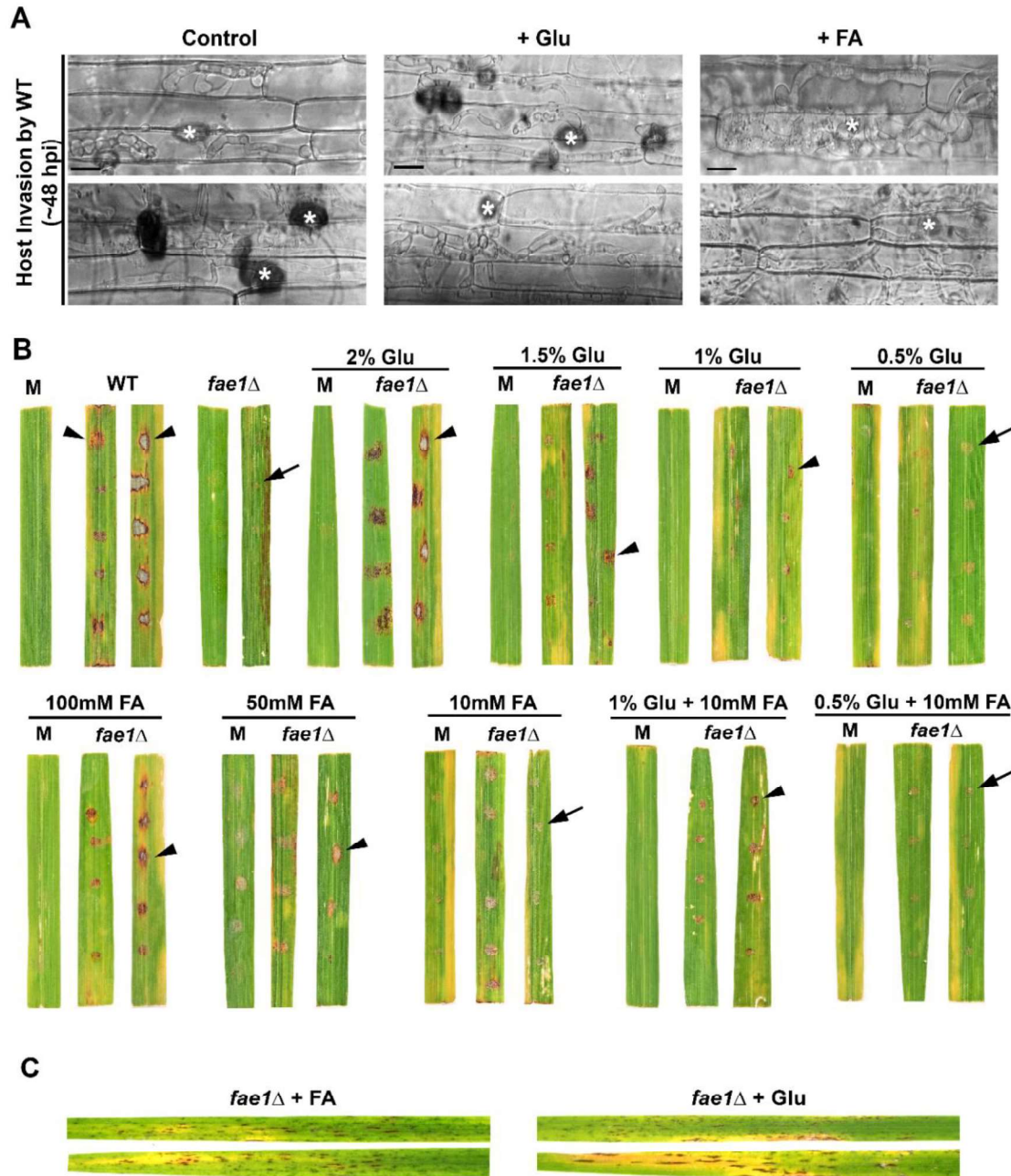


Figure 3.2.14. Assessment of *in vitro* host invasion and infection ability of the WT or *fae1* Δ in the presence or absence of different concentrations of glucose and/or ferulic acid. (A) Micrographs showing unaltered host invasion ability of the WT in the presence of 2% glucose or 100 mM ferulic acid exogenously added at 22 hpi. Scale bar, 10 μ m. (B) Infection ability of WT, *fae1* Δ or *fae1* Δ under different conditions were checked by drop-inoculation on detached rice leaves. Respective compounds were added at ~22 hpi. Disease outcome was recorded at 5-6 dpi. Arrowheads mark typical disease lesions, while arrows depict a very mild to moderate disease symptoms. M, mock inoculation with either plain water or the compound alone. (C) Whole-plant infection assay depicting blast disease outcome from the rice plants spray-inoculated with the *fae1* Δ mutant supplemented at 22 hpi with 2% glucose or 100 mM ferulic acid. The representative leaves were detached and photographed after 6 dpi.

4.5.4 Ferulic acid most likely serves as an energy/nutrient source for the blast fungus

During rice-*Magnaporthe* interaction, plants generate ROS response as a first line of defense, whereas fungus produces antioxidants to suppress such ROS response to enter the host plant, mainly for nutrient acquisition. Ferulic acid, a small phenolic compound, possesses an antioxidant property, while on the other hand it could also serve as an alternative or weak energy source (Black and Dix, 1976). Thus, it was tested whether the rescue of the *fae1* Δ mutant phenotype upon exogenous supply of ferulic acid was due to its antioxidant property and/or its role as an energy source.

To find out whether ferulic acid served as an antioxidant, rice leaf and sheath tissues were inoculated with the *fae1* Δ conidia followed by exogenous addition of 20 mM reduced glutathione (GSH), which is a known antioxidant, at ~22 hpi. However, unlike ferulic acid, exogenous addition of GSH could not rescue the *fae1* Δ mutant (Fig. 3.2.15A and 3.2.15B). Next, to check whether *M. oryzae* could utilize ferulic acid as an energy source, WT mycelial plug was inoculated onto basal medium containing glucose (positive control) or ferulic acid as the sole carbon source. Vegetative mycelial growth was then checked at 10 dpi. Indeed, it was found that *M. oryzae* WT grew on the basal medium supplemented with ferulic acid as the sole carbon source (Fig. 3.2.15C). This possibly explains how exogenous addition of ferulic acid could rescue the *fae1* Δ strain, most likely by providing energy to support the invasive growth rather than acting as an antioxidant. Moreover, this observation corroborates with the finding that supplementation of glucose, an easily utilisable carbon/energy source, also supported invasive growth of the mutant.

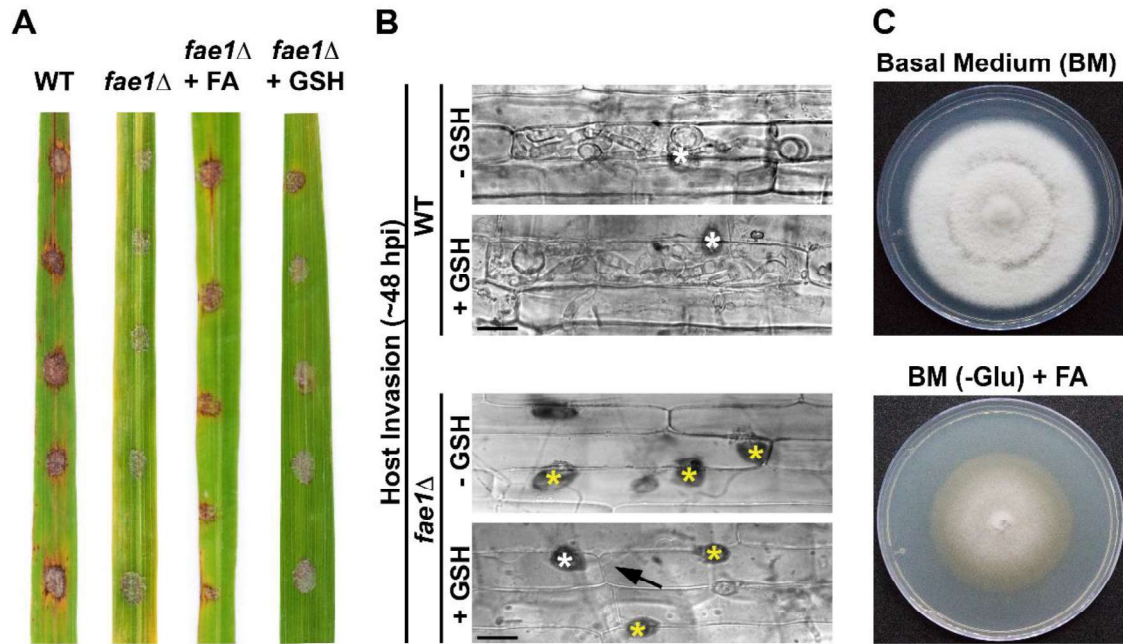


Figure 3.2.15. (A) Drop-inoculation assay showing infection ability (on detached rice leaves) of WT, *fae1Δ* or *fae1Δ* supplemented with 100 mM ferulic acid (FA) or 20 mM reduced glutathione (GSH). Images were taken at 6 dpi. (B) Leaf sheath inoculation assay showing host invasion ability of the WT or *fae1Δ* supplemented with 20 mM GSH, which was added at 22 hpi. The results were observed at 48 hpi. White and yellow asterisks mark the invading and non-invading appressoria, respectively. Arrow depicts invasive hypha restricted to the first host cell invaded. Scale bar, 10 μ m. (C) Vegetative growth of the WT *M. oryzae* on basal medium (BM) with 2% glucose or 0.01% ferulic acid. The images were taken at 10 dpi.

Overall, Fae in *M. oryzae*, similar to *A. niger*, likely acts in a concerted manner, on the esterified ferulic acid bridges in the plant cell wall to allow endo-xylanases and cellulases to work on the carbohydrates therein, releasing constituent sugar molecules and ferulic acid, which could act as the energy source during host invasion and colonisation (Fig. 3.2.16).

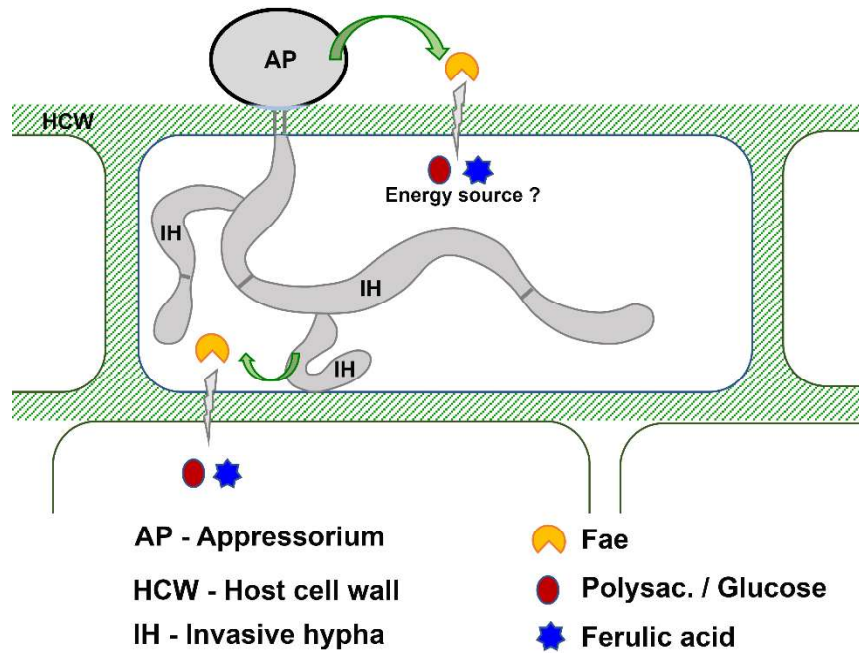


Figure 3.2.16. A proposed model of Fae1 function during pathogenesis in *M. oryzae*. Fae1, likely secreted along with other CWDEs, hydrolyses the plant cell wall to release ferulic acid and constituent carbohydrates during penetration of the first host cell and subsequent spread to the neighbouring cells. Released ferulic acid, the product of Fae enzyme action, and/or glucose, the breakdown product of cellulose, likely act as an energy source enabling successful host-invasion and colonization by the blast fungal pathogen.